

# 1 Fresh tephra deposits from the Tajogaite Volcano boost thermophile 2 proliferation and soil organic matter recovery

3

4 Sara Gutiérrez-Patricio<sup>1</sup>, Alba Gómez-Arias<sup>1</sup>, Pedro Nolasco-Jiménez<sup>1</sup>, Jorge Mataix-Solera<sup>2</sup>, Javier  
5 Martínez-Martínez<sup>3</sup>, Bruno Martínez-Haya<sup>4</sup>, Juana Vegas<sup>3</sup>, Nicasio T. Jiménez-Morillo<sup>1</sup>, Ana Z. Miller<sup>1,5</sup>

6

7 <sup>1</sup> Instituto de Recursos Naturales y Agrobiología de Sevilla (IRNAS-CSIC), Avda. Reina Mercedes 10, 41012, Seville, Spain

8 <sup>2</sup> Grupo de Edafología y Tecnologías del Medio Ambiente GETECMA. Departamento de Agroquímica y Medio Ambiente,  
9 Universidad Miguel Hernández, 03202 Elche, Alicante, Spain.

10 <sup>3</sup> Instituto Geológico y Minero de España (IGME-CSIC), Ríos Rosas 23, 28003 Madrid, Spain.

11 <sup>4</sup> BIO-MS group, Department of Physical, Chemical and Natural Systems, Universidad Pablo de Olavide, 41013, Seville,  
12 Spain.

13 <sup>5</sup> Hercules Laboratory, University of Évora, Palacio do Vimioso, 7000-809, Évora, Portugal.

14 Correspondence to: Nicasio T. Jimenez-Morillo ([ntjm@irnas.csic.es](mailto:ntjm@irnas.csic.es)) / Ana Z. Miller ([anamiller@irnas.csic.es](mailto:anamiller@irnas.csic.es))

15

16 **Abstract.** Tephra fallout deposition during volcanic eruptions overlays existing soils, profoundly altering their physical,  
17 chemical, and biological properties. This study investigates the impact of the newly deposited tephra blanket from the 2021  
18 Tajogaite eruption (La Palma Island) on the molecular composition of soil organic matter and microbial diversity across  
19 different soil horizons. A combination of 16S ~~and 18S~~ rRNA gene sequencing, pyrolysis-gas chromatography/mass  
20 spectrometry (Py-GC/MS), and elemental and isotope ratio mass spectrometry (EA/IRMS) was employed. Our results  
21 demonstrate that tephra deposits significantly modify the organic matter composition of the underlying soils, promoting  
22 microbial activity linked to the degradation and transformation of organic carbon and nitrogen compounds. The soil horizon  
23 directly beneath the tephra layer (horizon ~~O~~O) displayed a higher abundance of labile organic compounds and a reduced  
24 presence of recalcitrant compounds compared to the deeper horizons (A and Bw). This pattern is strongly associated with the  
25 predominance of thermophilic bacteria, which contribute actively to the breakdown of complex organic materials such as lignin  
26 and hydrocarbons, and drive key biogeochemical processes including nitrogen and carbon cycling. The continuous geothermal  
27 influence of nearby fumaroles further supports the persistence and ecological success of thermophilic communities in these  
28 volcanic soils. These findings underscore the critical role of volcanic activity not only in reshaping soil structure but also in  
29 enhancing soil fertility and resilience through microbial-mediated processes. Understanding these dynamics is essential for

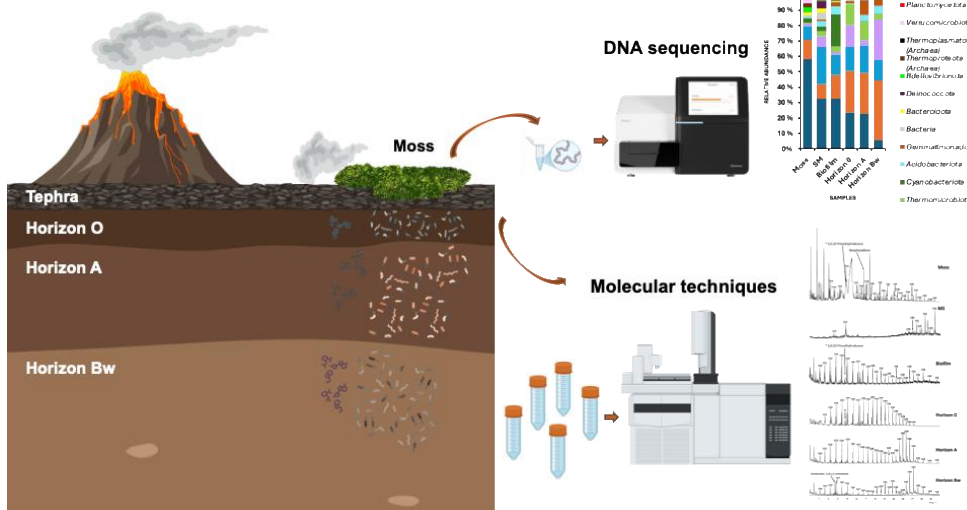
Código de campo cambiado

Código de campo cambiado

30 soil management and ecosystem recovery strategies in volcanic regions, providing new insights into the long-term effects of  
31 tephra deposition on soil health and the carbon cycle.

32

33 **Graphical abstract**



34

35

36

37 **1. Introduction**

38 The Tajogaite volcanic eruption, which began in September 2021 on La Palma Island (Canary Islands, Spain), was an  
39 extraordinary geological event that significantly transformed the local environment (Birnbaum et al., 2023; Troll et al., 2024).  
40 Over 85 days, the eruption released over 200 million cubic meters of lava and pyroclasts, burying over 1,200 hectares of land  
41 and displacing 7000 residents. The voluminous ashfall, with a complex tephra blanket reaching up to 2.5 m thick, profoundly  
42 impacted the ecosystem of La Palma and posed substantial challenges for local agriculture, infrastructure, and human health  
43 (Craig et al., 2016; Bonadonna et al., 2022, 2023; Birnbaum et al., 2023; Sánchez-España et al., 2023; Biass et al., 2024).  
44 According to these authors, the grain size of the tephra blanket varied during the eruption from lapilli >6 cm to very fine ash  
45 (<2 mm) that spread to La Gomera, El Hierro, Tenerife and Gran Canaria islands during the more explosive phases. Ashfall  
46 significantly impacted agricultural productivity (Sánchez-España et al., 2023; Taddeucci et al., 2023). The loss of fertile topsoil  
47 and the alteration of soil properties created long-term challenges for agricultural recovery and land use (Ustiatik et al., 2023).  
48 Volcanic tephra is a fine-grained unconsolidated deposit, highly reactive material that can considerably modify soil structure,  
49 chemistry, and biology (Nanzyo et al., 1993; Arnalds, 2013; Wygel et al., 2019). When deposited on existing soil layers, tephra  
50 can create a new surface horizon that introduces novel mineral substrates and interacts with soil organic matter (SOM),  
51 triggering complex chemical and biological transformations (Hayakawa et al., 2020; Wijesinghe et al., 2020; Peng et al., 2021).  
52 These changes can influence soil fertility, stability, and overall health by modifying nutrient availability, pH, and soil  
53 aggregation (Peng et al., 2021; De la Rosa et al., 2023). Additionally, the ash can act as a catalyst for the formation of new  
54 organic-mineral complexes, altering SOM decomposition pathways and the long-term sequestration of carbon and other  
55 essential nutrients (Nierop and Buurman, 2007; Hernández et al., 2012; Iwasaki et al., 2021). Understanding these processes  
56 is crucial, particularly in volcanic regions where soil resilience is key to ecosystem recovery.

57 Soil health is intrinsically linked to the composition and stability of SOM (Arias *et al.*, 2005), which consists of a diverse array  
58 of plant-derived, microbial, and fungal compounds (González-Pérez et al., 2004). Fresh tephra deposition in regions affected  
59 by volcanic activity can significantly alter the soil capacity to retain nutrients and support plant and microbial communities,  
60 ultimately influencing the trajectory of ecosystem recovery (Hernández et al., 2012; Yokobe et al., 2020; Muñoz et al., 2021).  
61 Furthermore, the interactions between volcanic ashfall and SOM can lead to the formation of polycyclic aromatic hydrocarbons  
62 (PAHs) and other condensed compounds (Nanzyo et al., 1993; Tomašek et al., 2021).

63 The effects of volcanic ash extend beyond physical and chemical changes; they also shape the microbial communities in soils  
64 (Zeglin et al., 2016; Yokobe et al., 2020; Chen et al., 2021). Microorganisms are highly sensitive to changes in soil properties,  
65 and ash deposition can create new niches that favour specific microbial taxa adapted to the altered conditions (Chen et al.,  
66 2021). This alteration in microbial diversity can have profound implications for soil function, influencing processes such as  
67 SOM decomposition, biogeochemical cycle of carbon and nitrogen, nutrient cycling, and the production of secondary  
68 metabolites (Campos et al., 2020; Gutierrez-Patricio et al., 2024).

69 Under the hypothesis that tephra deposits from volcanic eruptions can modify the microbiota and the organic matter  
70 composition of the underlying soils. This work aimed to investigate the impact of the Tajogaite volcanic eruption on the  
71 molecular and microbial diversity of an existing soil profile that has been covered by tephra deposits and delucidateelucidate  
72 its influence ion soil resiliency and ecosystem recovery capacity. Using advanced molecular and microbiological techniques,  
73 including pyrolysis-gas chromatography/mass spectrometry (Py-GC/MS), stable isotope analysis, and 16S and 18S-rRNA  
74 gene-sequencing, the soil profiles under recent ash deposition was were analysed to unravel how volcanic ash alters SOM  
75 quality and microbial community structure.  
76 The findings provide key insights into the mechanisms driving soil transformation following volcanic events and highlight the  
77 critical role of SOM and microbial dynamics in soil resilience and ecosystem recovery.

78

## 79 2 Material and Methods

### 80 2.1 Study site and sampling

81 The soil profile studied is located in the *Las Manchas* area of La Palma Island, within the region most affected by the 2021  
82 Tajogaite volcanic eruption. La Palma Island, part of the Canary Islands archipelago and located approximately 400 km west  
83 of the African coast, has a total area of 708 km<sup>2</sup> and is one of the youngest in the archipelago, formed during the last 1.8 million  
84 years (Hoernle et al., 2009). La Palma Island shows the most complete record of the evolution of an oceanic volcanic island,  
85 starting from the Pliocene submarine basal complex, the metamorphism originated by magmatic intrusion, the building of a  
86 Quaternary volcanic edifice, and giant landslides and intense erosion that defines the final morphology of Caldera de  
87 Taburiente. Volcanism displaced to a N-S elongated polygenetic Cumbre Nueva volcanic ridge that has developed over the last  
88 c. 125 ka (Carracedo et al., 2001; Sánchez-España et al., 2023) being the most active area of this island (Longpre & Felpeto,  
89 2021).

**Con formato:** Fuente: Cursiva

90 The 2021 Tajogaite volcanic eruption, which began on September 19 and lasted for 85 days, emitted over 200 million cubic  
91 meters of lava and pyroclastic materials, creating extensive lava flows that covered approximately 1,200 hectares and extended  
92 into the Atlantic Ocean, forming two new lava deltas (Ferrer et al., 2023). The pyroclastic materials deposited during this  
93 eruption ranged in size from fine ash to large lapilli and created a stark contrast with the pre-existing landscape (Bonadonna  
94 et al., 2022; Ferrer et al., 2023). The eruption also introduced a tephra blanket, up to 3 m thick in areas close to the volcanic  
95 cone, that overlies the native soils (Bonadonna et al., 2023).

**Con formato:** Fuente: Cursiva

96 The study site is located in the *Las Manchas* area (Los Llanos de Aridane municipality), situated on the western slopes of the  
97 Cumbre Nueva Ridge (Fig. 1A). Before the eruption, the soils in this area were classified as Typic Ustivitrands (Soil Survey  
98 Staff, 2022). These soils typically exhibit a sandy loam texture, low bulk density, and a high degree of aggregation, particularly  
99 in the surface horizons, which are enriched with organic matter (see Table S1).

100 Following the eruption, the pre-existing soils in the study area were buried under a 20 cm thick layer of tephra and ash. Two  
101 years after the event, mosses colonized the tephra deposit surface, and biofilms developed at the soil-tephra interface (Fig.  
102 1B). Sampling included the collection of moss growing on the fresh tephra (MOSS), the tephra layer directly beneath the moss  
103 cover (moss substrate, MS), a dark green biofilm on horizon  $0\Theta$  (Biofilm), and three soil horizons:  $0\text{--}2\text{ cm}$  (Horizon O),  $0\text{--}2\text{ cm}$   
104 (em),  $A\text{ (2--10 cm)}$  (Horizon A) and  $Bw\text{ (10--20 cm)}$  (Horizon Bw) (Fig. 1B). All samples analyzed in this study were composite  
105 samples, generated by collecting five subsamples per sample type across distinct sampling points and/or soil horizons, followed  
106 by thorough homogenization and pooling into a single representative mixture. This volcanic ash-derived soil profile was  
107 located near steam-emitting fumaroles, in a sector with a high temperature anomaly in the soil. These fumaroles vent water  
108 vapour as the main component and other chemical species, such as  $\text{SO}_2$ ,  $\text{H}_2\text{S}$ ,  $\text{HCl}$ , and  $\text{CO}$  gases up to 20.7, 17.7, >30.0 and  
109 19.5 ppm, respectively, at temperatures higher than the ambient (Campeny et al., 2023; Martínez-Martínez et al., 2023).  
110 This site provides a unique opportunity to study the interactions between fresh tephra deposits and the underlying soil,  
111 particularly their effects on soil structure, organic matter composition, and microbial communities.  
112 All samples were collected using sterile tools, such as spatulas or individually wrapped disposable scoops, to avoid  
113 contamination, and all samples were immediately placed into sterile Whirl-Pak bags. The samples were kept on ice during  
114 transportation to the laboratory for subsequent analysis. Subsamples of each material were used for DNA-based analysis,  
115 carbon and nitrogen elemental and isotope analysis, and molecular composition.  
116 The environmental conditions of the sampling area were monitored by installing a temperature and relative humidity sensor  
117 (HOBO MX2301A, ONSET®, Fig. S1A and B) near the fumarole vent to assess the temperature of the water vapour emissions  
118 from the fumarole. This sensor took measurements every hour for one year.  
119



120  
121 **Figure 1: A) Location of the soil profile under tephra blanket in Las Manchas (La Palma, Spain), and B) sampling area of the volcanic**  
122 **ash-derived soil profile comprising  $m\text{Moss}$ , moss substrate (MS),  $B\text{biofilm}$  located in the horizon O, and three horizons (O and**  
123 **Bw).**  
124

125 **2.2 Carbon and nitrogen elemental and isotope analysis**

126 The compositional analysis of organic carbon and nitrogen in both pyroclastic materials and soil samples was carried out using  
127 a Flash 2000 HT Elemental Micro-analyzer connected to a Thermal Conductivity Detector (EA/TCD; Thermo Scientific in  
128 Bremen, Germany). Samples, ranging in weight from 5 to 10 milligrams, were processed in duplicate ( $n = 2$ ) following a  
129 decarbonization treatment as outlined by Jiménez-Morillo et al., (2016, 2020a). The calibration of carbon and nitrogen content  
130 employed certified standards such as acetanilide, nicotinamide, and aspartic acid, provided by Thermo Scientific, Bremen,  
131 Germany. The carbon and nitrogen isotope ratios ( $^{13}\text{C}/^{12}\text{C}$  and  $^{15}\text{N}/^{14}\text{N}$ ) were determined using an Elemental Analyzer  
132 connected to a Thermo Fisher Delta V Advantage Isotope Ratio Mass Spectrometer (EA/IRMS), following the method  
133 described by (Jiménez-Morillo et al., 2020b). These procedures were conducted at the Stable Isotope Laboratory - MOSS at  
134 IRNAS-CSIC (Spain). Isotope values are expressed in delta ( $\delta$ ) notation in parts per thousand (‰) relative to certified standards  
135 set by the International Atomic Energy Agency (IAEA), with a standard deviation for bulk  $\delta^{13}\text{C}$  of  $\pm 0.05\text{ ‰}$  and  $\delta^{15}\text{N}$  of  $\pm 0.1$   
136 ‰. Duplicate analyses were performed for samples and standards ( $n = 2$ ).

137

138 **2.3 Analytical pyrolysis (Py-GC/MS)**

139 The analytical pyrolysis (Py-GC/MS) technique was composed of i) a double-shot pyrolyzer, model 3030D (Frontier  
140 Laboratories, Japan), set at 500 °C; ii) an Agilent 6890N gas chromatograph, and iii) an Agilent 5973 MSD (mass selective  
141 detector) mass spectrometer, operating at an electron impact energy of 70 eV. The chromatographic separation involved an  
142 HP-5MS UI capillary column (30 m length, 0.25 mm internal diameter, 0.25 μm film thickness) with a helium flow rate of 1  
143 mL min<sup>-1</sup>. The sample injection was conducted in splitless mode at 250 °C, and the temperature program was adopted from  
144 protocols described by Jiménez-Morillo et al., (2020a). Ion fragments ranging from 50 to 550 m/z were recorded, and  
145 compound identification was conducted by comparison with virtual spectral libraries, such as the NIST20 and Wiley7. The  
146 molecular compounds released by Py-GC/MS were categorized into the eight biogenic families proposed by Jiménez-Morillo  
147 et al (2016a): unspecific aromatic compounds (ARO), polysaccharides (POL), peptides (PEP), lignin (LIG), lipids (LIP),  
148 nitrogen-containing compounds (N-comp), polycyclic aromatic hydrocarbons (PAHs), and steranes (STR). Chromatographic  
149 peak area >0.2% of the total chromatographic area was not taken into account. For a detailed study of homologous series of *n*-  
150 alkanes and *n*-alken-2-ones, single ion monitoring of specific fragments - specifically ions with m/z 57 and m/z 59, respectively  
151 - was adopted.

152

153 **2.4. DNA extraction and 16S rRNA gene amplicon sequencing**

154 [Genomic DNA was extracted from 250 mg of each sample \(n = 6\) using the DNeasy PowerSoil Pro Kit \(Qiagen, Germany\)](#)  
155 [following the manufacturer's instructions. DNA concentration was quantified using a Qubit 4.0 fluorometer \(Invitrogen\).](#)

**Con formato:** Fuente: Sin Negrita

156 The V3–V4 hypervariable region of the prokaryotic 16S rRNA gene was amplified using the universal primers 341F (5'-  
157 CCTACGGGNGGCWGCAG-3') and 805R (5'-GACTACHVGGGTATCTAATCC-3') with Illumina overhang adapter  
158 sequences, following Klindworth et al. (2013). Amplicon libraries were sequenced on an Illumina MiSeq platform using 2 ×  
159 250 bp paired-end chemistry. Library preparation and sequencing were performed by Novogene Sequencing Services (China).  
160 Raw sequencing reads were deposited in the NCBI Sequence Read Archive (SRA) under accession PRJNA1192049.

161

## 162 2.5. Bioinformatic processing and diversity analyses

163 Raw paired end reads were processed in QIIME 2 (v2024.5) (Bolyen et al., 2019). Primer sequences were removed prior to  
164 denoising, and reads were quality filtered, denoised, and merged using the q2\_dada2 plugin (Callahan et al., 2016) to generate  
165 an amplicon sequence variant (ASV) feature table; chimeric sequences were removed using the consensus method  
166 implemented in DADA2. Taxonomy was assigned using a Naïve Bayes classifier trained for the V3–V4 region against the  
167 SILVA reference database (release 138) (Quast et al., 2013).

Con formato: Fuente: Sin Negrita

168 The alpha and beta diversity analyses were calculated using the QIIME 2 version 2024.5 to quantify the microbial diversity  
169 within each sample. Alpha diversity metrics were computed to summarize within-sample diversity. Beta diversity was assessed  
170 using Bray–Curtis (abundance-based) and Jaccard (presence/absence) dissimilarities, and community patterns were visualized  
171 by principal coordinates analysis (PCoA). Given the limited number of samples ( $n = 6$ ) and the absence of biological replication  
172 per sample type, results were interpreted descriptively to highlight patterns rather than to perform formal hypothesis testing  
173 among groups.

Con formato: Fuente: Sin Negrita, Resaltar

## 174 2.4 DNA extraction and sequencing

175 Genomic DNA was extracted from 250 mg of each of the five samples using the DNeasy PowerSoil Pro Kit (Qiagen, Germany)  
176 following the manufacturer's instructions. The DNA was quantified using a Qubit 4.0 fluorometer (Invitrogen).  
177 The extracted DNA was analyzed through next generation sequencing (NGS), targeting the V3–V4 hypervariable region of the  
178 16S rRNA gene for prokaryotes. Amplicons were sequenced using the Illumina MiSeq platform to generate 250 bp paired-end  
179 raw reads, performed by Novogene Sequencing Services (China).

Con formato: Fuente: Sin Negrita

180 Raw amplicon sequence data were processed using QIIME 2 version 2024.5 (Bolyen et al., 2019). The table of Amplicon  
181 Sequence Variants (ASVs) was generated using DADA2, following its instructions (Callahan et al., 2016). Taxonomic  
182 classification was assigned using the SILVA reference database, version 138 (Quast et al., 2013). Alpha diversity analysis was  
183 calculated in QIIME2 version 2024.5 (Bolyen et al., 2019) to quantify the microbial diversity within each sample.  
184 The raw reads were deposited in the NCBI Sequence Read Archive (SRA) database under accession number PRJNA1192049.

## 185 2.5. Bioinformatic processing

186 Raw paired-end reads were processed using QIIME 2 (v2024.5) (Bolyen et al., 2019). Primer sequences were removed prior  
187 to denoising to prevent primer-derived artifacts and to improve read merging. Reads were then quality filtered and denoised

188 using the q2-dada2 plugin (Callahan et al., 2016), which infers exact amplicon sequence variants (ASVs) by modeling  
189 sequencing errors and resolving unique biological sequences. Forward and reverse reads were merged to reconstruct the full  
190 V3–V4 amplicon, generating an ASV feature table for downstream ecological analyses. Chimeric sequences produced during  
191 PCR amplification were identified and removed using the consensus approach implemented in DADA2, reducing spurious  
192 diversity. Taxonomy was assigned with a Naïve Bayes classifier trained on the V3–V4 region against the SILVA reference  
193 database (release 138) (Quast et al., 2013), ensuring that taxonomic classification was optimized for the targeted amplicon  
194 region.

195

## 196 2.6. Diversity and statistical analyses

197 Alpha diversity analyse was computed in QIIME 2 (v2024.5). Alpha diversity was calculated to summarize within-sample  
198 diversity using richness and diversity indices (e.g., observed ASVs, Chao1, Shannon, and Simpson, as appropriate). To aid  
199 interpretation of the ordination, we produced a PCoA biplot by projecting (i) geochemical/pyrolytic descriptors (e.g.,  
200 compound-class abundances from pyrolysis and elemental contents) and (ii) the relative abundances of dominant microbial  
201 phyla onto the same ordination space. Vectors (arrows) represent the direction of increasing values for each variable and their  
202 strength of association with the ordination axes (longer vectors indicate stronger relationships). This combined representation  
203 was used to highlight which chemical pools and microbial groups co-varied across samples and to identify the main gradients  
204 driving separation along PCo1 and PCo2.

205

## 206 **3 Results and discussion**

### 207 **3.1 Elemental and isotope composition of carbon and nitrogen**

208

209 **Table 1: Isotope and elemental composition of nitrogen (N) and carbon (C) of *M*moss, moss substrate (MS), *B*biofilm  
210 and three soil horizons (O, A and Bw). Significant ( $p < 0.05$ ) differences between samples are indicated by different  
211 letters ("one-way ANOVA"; means compared to the Tukey test,  $p = 0.05$ ).**

Sample	$\delta^{15}\text{N}$ (‰, V-Air)	$\delta^{13}\text{C}$ (‰, VPDB)	N (%)	C (%)
Moss	-5.1±0.4d	-28.5±0.1b	0.62±0.12b	12.53±1.69c
MS*	5.0±2.9bc	-24.3±1.6ab	3.17±0.80ab	28.71±4.53bc
Biofilm	1.9±0.9c	-28.4±3.5ab	4.37±1.86a	38.59±16.65ab
Horizon O	7.9±0.5b	-29.2±1.6b	4.99±0.78a	55.27±8.09a
Horizon A	6.0±0.4bc	-24.8±1.3ab	1.60±0.51b	17.60±3.39bc
Horizon Bw	16.6±3.1a	-23.5±0.4a	0.95±0.87b	8.65±4.48c

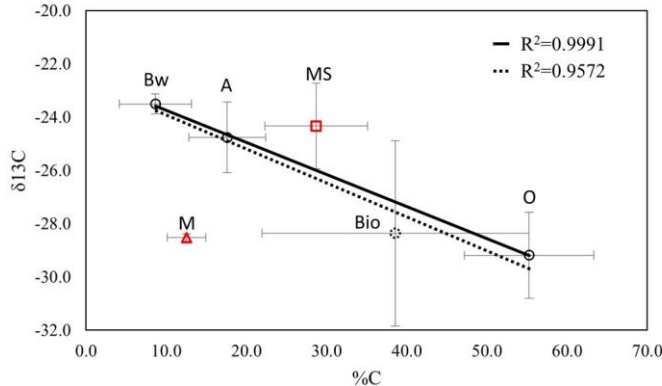
212 \*MS = moss substrate

213

Con formato: Fuente: Negrita

214 Table 1 depicts the average values and standard deviations of the elemental and isotope composition of carbon (C) and nitrogen  
215 (N) in M<sub>m</sub>oss, moss substrate (MS), B<sub>b</sub>iofilm, and three soil horizons (Horizon 0O, A, and Bw). Horizon 0O samples exhibited  
216 the highest average of C and N content ( $55.3 \pm 8.1$  and  $5.0 \pm 0.8$ , respectively), which may be associated with a noticeable root  
217 layer (Fig. 1). The B<sub>b</sub>iofilm also shows notable C and N content (38.59% and 4.37%, respectively) and is located in Horizon  
218 O. These values are typical of biofilms, and its ratio C/N close to 9 (8.83 on average) indicates that the biofilm was found in a  
219 healthy state. Previous studies have shown that biofilms with C/N ratio close to 9 have higher concentrations of carbohydrates  
220 and proteins in the biofilm and a significant upregulation of the Quorum Sensing genes (Ramos et al., 2023).  
221 In contrast, the C and N values in the horizons A ( $17.6 \pm 3.39$  and  $1.6 \pm 0.51$ , respectively) and Bw ( $8.65 \pm 4.48$  and  $0.95 \pm$   
222 0.87, respectively) were consistent with those reported in different soil types, the concentration of both elements in horizon A  
223 is three-fold of those found in B (Girona-García et al., 2018; Jiménez-Morillo et al., 2020a). These findings align with previous  
224 studies indicating a decline in C and N content with increasing soil depth. For M<sub>m</sub>oss and moss substrate (MS), the higher C  
225 content in MS compared to M<sub>m</sub>oss could be attributed to the presence of numerous small moss roots, which form a three-  
226 dimensional network that aggregates and stabilizes lapilli grains. Additionally, the presence of root exudates, rich in C and N  
227 compounds, may contribute to this remarkable concentration of organic compounds. This is the first indication of soil re-  
228 generation after the volcanic eruption of Tajogaite, which reveals the importance of moss in this process. Previous studies  
229 about the colonization of soils affected by volcanic activity highlight the abundance of photosynthetic organisms, including  
230 moss, as pioneer colonizers (Smith, 1984; Ingimundardóttir et al., 2014; Vilmundardóttir et al., 2018; Dragone et al., 2023).  
231 Regarding the C isotope composition, all samples exhibited  $\delta^{13}\text{C}$  values within the typical range for C<sub>3</sub> plants (between -25 ‰  
232 and -35 ‰ (Katsumi et al., 2015; Ghezzi and Jimenez-Morillo et al., 2024). However, significant differences were observed  
233 among the samples. Moss, Horizon O, and B<sub>b</sub>iofilm displayed the most negative  $\delta^{13}\text{C}$  values ( $-28.5 \pm 0.1$ ,  $-28.4 \pm 3.5$ ,  
234 and  $-29.2 \pm 1.6$ , respectively), which reflected the presence of fresh organic matter (Jiménez-Morillo et al., 2020b). In  
235 contrast, samples from the A and Bw soil horizons and the moss substrate (MS) were enriched in <sup>13</sup>C (Table 1). This trend has  
236 also been observed by Girona-García et al., (2018) in soil profiles under pine and beech forests, where deeper horizons  
237 exhibited higher  $\delta^{13}\text{C}$  values. Such <sup>13</sup>C-enrichment in soil samples is often associated with more humified organic matter  
238 (Jiménez-Morillo et al., 2020b). For the MS ( $\delta^{13}\text{C} = -24.3 \pm 1.6$ ), the observed <sup>13</sup>C-enrichment may be attributed to i) the  
239 heavier isotope signature of root exudates compared to other organic compounds commonly found in soil samples (Girona-  
240 García et al., 2018), and ii) microbial activity linked to diverse families of microorganisms (Jiménez-Morillo et al., 2020b;  
241 Miller et al., 2022; San-Emeterio et al., 2023). In addition, Horizons A and Bw have similar  $\delta^{13}\text{C}$  values ( $-24.8 \pm 1.3$  and  $-23.5$   
242  $\pm 0.4$ , respectively) to the MS, which is mainly composed of tephra. This could be indicative of the volcanic origins of the  
243 paleo soil (Horizons A and B) (Carracedo et al., 2022) and the importance of lapilli, among other volcanic materials from  
244 previous eruptions, in the carbon cycle during the soil formation (Matus et al., 2014 and references therein).

245 A key finding is the strong negative correlation observed between  $\delta^{13}\text{C}$  values and C content across the different soil horizons  
 246 and the B<sub>biofilm</sub> (Fig. 2). This trend is particularly pronounced in the soil horizon samples ( $R^2 = 0.9991$ ; solid line). However,  
 247 when the B<sub>biofilm</sub>-sample is included, the correlation weakens slightly ( $R^2 = 0.9572$ ; dashed line).



248  
 249 **Figure 2: Plot of average (n=3)  $\delta^{13}\text{C}$  vs %C of M<sub>moss</sub> (red triangle), moss substrate (MS, red square), B<sub>biofilms</sub> (black dashed circle)  
 250 and soil horizons O, A and Bw (open black circles) with linear regression of horizons (solid line) and including biofilms (dashed line).**  
 251

252 This negative correlation between  $\delta^{13}\text{C}$  and C content has been previously described in soils worldwide. In all cases, this trend  
 253 has been attributed to either the decomposition of organic matter, the fractionation by microbial activity or the shift of a  
 254 predominant contribution from plants to microorganisms in the residual organic matter as it progresses through the soil  
 255 horizons (Ågren et al., 1996; Volk et al., 2018; Ehleringer et al., 2000; Krüger et al., 2024). The microbial activity may process  
 256 fresh organic matter, leaving behind evolved (humified) material with a heavier isotope. This alteration may also reduce the C  
 257 content due to microbial respiration. A similar pattern has been observed in the isotope composition of highly humified  
 258 (evolved) organic matter associated with very fine sand particles in shallow soil layer (Jiménez-Morillo et al., 2020a), which  
 259 may confirm the influence of microorganisms in the humification process of fresh organic matter. However, the M<sub>moss</sub> and  
 260 the tephra collected under the moss (MS) did not correlate with the soil. This is probably because the samples were collected  
 261 shortly after the volcanic eruption that accumulated the tephra over the previous soil (Horizon O). Therefore, the C cycle of  
 262 this interface was still in an early stage of the andisol formation process, preventing the observation of statistical correlations  
 263 between the soil samples and the tephra.

264 Regarding the nitrogen isotope composition ( $\delta^{15}\text{N}$ ), the M<sub>moss</sub> sample exhibited the lowest  $\delta^{15}\text{N}$  value (Table 1), a typical  
 265 characteristic for mosses (Zechmeister et al., 2008). In contrast, the other samples displayed positive  $\delta^{15}\text{N}$  values (Table 1).  
 266 For the MS sample, the <sup>15</sup>N-enrichment and their statistical similarity with  $\delta^{15}\text{N}$  values observed in the soil and biofilm samples  
 267 suggest that it could be derived from the activity of certain microorganisms, such as cyanobacteria, that utilize nitrogen-derived  
 268 compounds excreted by the moss roots (Carrell et al., 2022). In addition, the deepest soil sample (Horizon Bw) showed the

269 highest  $\delta^{15}\text{N}$  enrichment, which could be associated with denitrification processes (Girona-García et al., 2018). While  
270 humification is well known to cause  $^{15}\text{N}$ -enrichment, particularly in forest soils (Szpak, 2014),  $^{15}\text{N}$ -depletion can occur during  
271 the uptake of inorganic N by vegetation (Högberg, 1997). Therefore, the observed trend can be best explained by the alteration  
272 of biomass by heterotrophic organisms, which produce  $^{15}\text{N}$ -depleted compounds while progressively enriching the remaining  
273 biomass with  $^{15}\text{N}$  over time (Billings and Richter, 2006; Makarov, 2009; Szpak, 2014; Girona-García et al., 2018).

274

### 275 3.2 Molecular composition of organic fraction

276 The use of analytical pyrolysis (Py-GC/MS) has revealed remarkable molecular differences between soil, tephra, Bbiofilm,  
277 and Moss samples (Fig. 3). The Moss sample is rich in organic compounds, particularly lipids (31.56%) and  
278 polysaccharides (29.75%), aligning with findings from previous studies (Klavina et al., 2015; Petkova et al., 2023). Among  
279 the lipid compounds identified were essential oils, such as  $\alpha$ -Terpinene and Phytol, *n*-alkanes (e.g., heptadecane, heneicosane;  
280 Klegin et al., 2023) and *n*-alkanoic acids (e.g., 9,12,15-Octadecatrienoic acid, 13-Eicosenoic acid, 22-Tricosenoic acid; Yucel,  
281 2021; Klegin et al., 2023). Polysaccharides in bryophytes play an important role in the chemical evolution of vegetation and  
282 assist as structural components, which are also assumed to contribute to bryophyte stress tolerance (Klavina et al., 2015). In  
283 this study, the identified polysaccharides were primarily furans (e.g., 2(5H)-Furanone, 5-methyl-, 2-Furancarboxylic acid,  
284 methyl ester, 3-Furaldehyde) and levoglucosan ( $\beta$ -D-Glucopyranose, 1,6-anpah). However, due to dehydration and molecular  
285 restructuring during pyrolysis, complete identification of polysaccharides is not feasible (González-Pérez et al., 2016). The  
286 molecular analysis also revealed a significant presence of non-specific aromatic compounds (13.60%) and peptide compounds  
287 (11.69%). Among the aromatic compounds, phenol derivatives such as Phenol, 2-methyl-, Phenol, 2,3-dimethyl-, 1,2-  
288 Benzenediol, and Phenol, 2,3,5-trimethyl were prominent. These phenolic compounds are considered critical in early plant  
289 evolution, particularly in moss growth and cuticle permeability, which were key for adaptation to terrestrial environments  
290 (Renault et al., 2017). Such phenolic compounds are precursors to lignin, synthesized by the phenylpropanoid pathway, which  
291 strengthens cell walls, aids in water transport, and supports upright growth (Fraser and Chapple, 2011). Peptide-derived  
292 compounds were also found, with their primary function being the defence of mosses against environmental stressors such as  
293 drought and high temperatures (Ren et al., 2024). Additionally, these peptides provide resistance against microbial pathogens  
294 (Valeeva et al., 2022). Plants produce a range of bioactive metabolites, peptides, and small molecules that contribute to defence  
295 mechanisms and microbial resistance (Valeeva et al., 2022). In addition, peptide compounds are crucial regulators of ecosystem  
296 function because they may provide as direct supplies of nutrients for soil microorganisms and plants (Wang et al., 2023).  
297 Only a few organic compounds were identified in the MS samples, mainly high molecular weight alkyl lipids (*n*-alkanes) and  
298 sterols, being the second the dominant group (65%). Key sterols detected include Stigmastan-3,5-dien, Campesterol, and  $\gamma$ -  
299 Sitosterol, also found in the Moss samples (Table S2). The presence of Campesterol and  $\gamma$ -Sitosterol may indicate an input  
300 of organic matter from the moss via rhizoid exudates. Sterols are crucial for various plant physiological processes, not only

301 supporting cell membrane structure and fluidity but also acting as hormone precursors and playing a role in responses to biotic  
302 and abiotic stress (Valitova et al., 2016; Cabianca et al., 2021). In addition, the presence of high molecular weight alkyl  
303 compounds, originating from epicuticular waxes, supports the hypothesis that there is a direct input of organic material from  
304 the moss to the substrate (tephra). The  $\delta^{13}\text{C}$  value observed in this sample does not align with the molecular composition  
305 identified by Py-GC/MS, as the detected compounds usually exhibit a markedly negative isotope signature (Park and Epstein,  
306 1961; San-Emeterio et al., 2023). However, the observed  $^{13}\text{C}$ -enrichment in this sample against the moss could be attributed  
307 to low-molecular-weight polysaccharide-derived compounds undetected by this analytical technique.

308 The Bbiofilm sample collected from Horizon 0Ω consists mainly of lipids (40.54%), non-specific aromatic compounds  
309 (38.36%), polysaccharides in the form of furans (13.08%), and peptides (8.02%). This molecular composition aligns perfectly  
310 with the main molecular composition found in Bbiofilm samples analyzed in different volcanic regions (Miller et al., 2020;  
311 Ghezzi and Jiménez-Morillo et al., 2024; Palma et al., 2024). The lipid composition is mainly dominated by *n*-alkane/alkene  
312 pairs with different proportions, which will be discussed in the section 3.3.1.

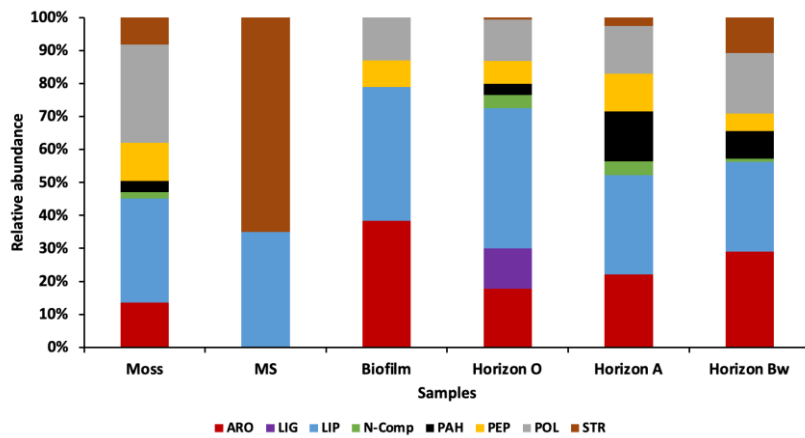
313 The Horizon 0Ω sample is dominated by lipid compounds (42.43%), mainly alkyl compounds (*n*-alkane/alkene pairs and *n*-  
314 alkanoic acids), followed by aromatic moieties (17.80%) and polysaccharides (12.57%). In addition, this is the only sample  
315 with a relatively high concentration of methoxyphenols, i.e., lignin-derived compounds (12.18%). The abundance of alkyl  
316 compounds suggests the existence of different organic fractions from distinct origins: i) organic matter from pre-eruption  
317 vegetation, also indicated by the  $\delta^{13}\text{C}$  of the Horizon 0Ω sample ( $-29.2 \pm 1.6$ ) typical of  $\text{C}_3$  plants, ii) the degradation of lipid  
318 membranes from microorganisms induced by the deposition of tephra during the Tajogaite volcanic eruption, and iii) highly  
319 evolved organic matter from post-eruption microbial activity in the soil (Jiménez-Morillo et al., 2017; Bull et al., 2000;  
320 Jiménez-Morillo et al., 2016b; Leal and Jimenez-Morillo et al., 2023). In contrast, the presence of lignin- and polysaccharide-  
321 derived compounds probably indicates the recent input of herbaceous/shrubby plant material (Fig. 1). It could also stem from  
322 root exudates of vegetation present before the ash deposition, supported by the high concentration of roots in the Horizon 0Ω  
323 (Fig. 1). Lignin compounds, particularly from the guaiacol and syringol groups, confirm a contribution of tree-derived organic  
324 matter (San-Emeterio et al., 2023). However, the greater abundance of guaiacol over syringol suggests ongoing microbial  
325 degradation activity, as syringol is more easily degraded by microorganisms (San-Emeterio et al., 2023). Additionally,  
326 condensed compounds (PAHs) were found in the shallow horizon. This could be generated by: i) ancient fires with particles  
327 trapped in the soil layers (Jiménez-Morillo et al., 2016b), ii) high-temperature vapour emissions, from volcanic fracture,  
328 leading to defunctionalization and condensation of polar aromatic compounds (Capaccioni et al., 1995) or, iii) microbial  
329 activity. Several pathways have been described for hydrocarbon synthesis by microorganisms (Ladygyna et al., 2006 and  
330 references therein). Some of these biogenic PAHs have been detected in forest soil (Kraus et al., 2005) with high degradation  
331 of lignin, in peatlands and wetlands (Wakeham et al., 2016), where organic matter accumulates and transforms slowly, and in

332 lake and marine sediments (Love et al., 2021), where microbial activity and anoxic conditions promote the polymerization of  
333 aromatic compounds.

334 The two deepest Horizons (A and Bw) of the soil profile share a similar molecular composition, dominated by non-specific  
335 aromatic compounds, lipid compounds (mainly *n*-alkane/alkene pairs), polysaccharides and peptides, with a complete absence  
336 of lignin molecules. This pattern has been observed in forest soils across the Iberian Peninsula (Aznar et al., 2016; Jiménez-  
337 Morillo et al., 2016a; De la Rosa et al., 2019), indicating the presence of microbial-derived compounds and linked to high  
338 microbial activity (Jiménez-Morillo et al., 2018). The abundance of non-specific aromatic compounds may also result from  
339 fungal degradation of plant lignins (Kellner et al., 2014). However, important differences include a higher proportion of  
340 condensed compounds (PAH = 15.17%) in the upper Horizon, while the deeper horizon has more sterane compounds (10.76%).

341 In the Horizon A, highly condensed PAHs, such as phenanthrene and pyrene suggest the presence of pyrogenic material, usually  
342 associated to organic matter combustion (González-Pérez et al., 2014; Miller et al., 2020, 2022). In contrast, the deeper Horizon  
343 only contains branched naphthalene compounds, possibly due to lower-intensity fires or microbial degradation of condensed  
344 compounds by thermophiles (Musat et al., 2009; Mohapatra and Phale, 2021). In the sterane family, the deeper Horizon (Bw)  
345 contains Stigmastan-3,5,22-triene, Ergosta-4,6,22-trien-3-ol, and Friedelan-3-one. These plant- and fungi-synthesized  
346 compounds are well-preserved in deeper layers due to their stability (Kristan and Rižner, 2012), with clear accumulation in the  
347 lower horizons, while they are almost absent in the Horizon 0O and the Bbiofilm (Fig. 3).

348

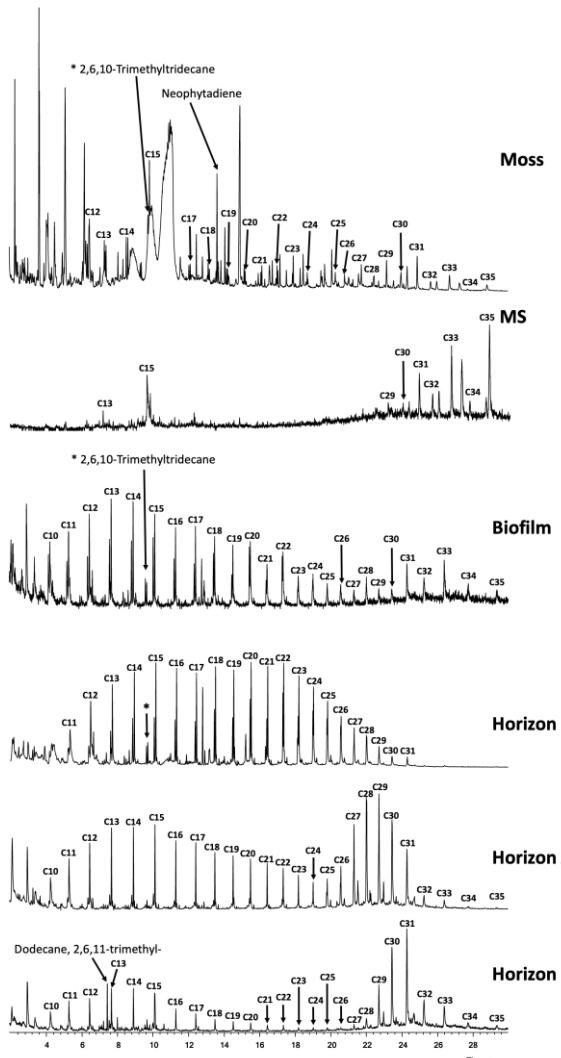


349

350 Figure 3: Relative abundance (%) of the main organic families identified by Py/GC/MS from Mmoss, moss substrate (MS), Bbiofilm,  
351 and soil horizons (O, A, Bw) samples. The main organic families are: unspecific aromatic compounds (ARO), polysaccharides (POL),  
352 peptides (PEP), lignin (LIG), lipids (LIP), nitrogen-containing compounds (N-comp), polycyclic aromatic hydrocarbons (PAHs), and  
353 steranes (STR).

354

## 355 3.3. Lipid analysis by Py-GC/MS

356 3.3.1. *n*-Alkanes

357

358 Figure 4: *n*-alkane (m/z 57) distribution obtained by direct pyrolysis (Py-GC/MS) of Mmoss, moss substrate (MS), Bbiofilms and  
 359 soil horizons (O, A and Bw) samples.

360

361 The *n*-alkane series were identified using m/z 57 in the selected-ion-monitoring (SIM) chromatogram (Fig. 4). Chain lengths  
 362 ranged from C<sub>10</sub> to C<sub>35</sub>, reflecting various organic matter sources (Jiménez-Morillo et al., 2017). In the Mmoss sample, a  
 363 bimodal distribution was observed with peaks at *n*-pentadecane (C<sub>15</sub>) and *n*-hentriacontane (C<sub>31</sub>), with odd-chain *n*-alkanes

364 predominating, especially in longer chains ( $>C_{25}$ ). This suggests *n*-alkanes from moss epicuticular waxes, with a peak at *n*-  
365 hentriacontane (Schwark et al., 2002). The presence of low-molecular-weight (LMW) *n*-alkanes ( $<C_{20}$ ) may point to associated  
366 microorganisms, as LMW *n*-alkanes typically originate from microbial cell walls (Jiménez-Morillo et al., 2017, 2022).

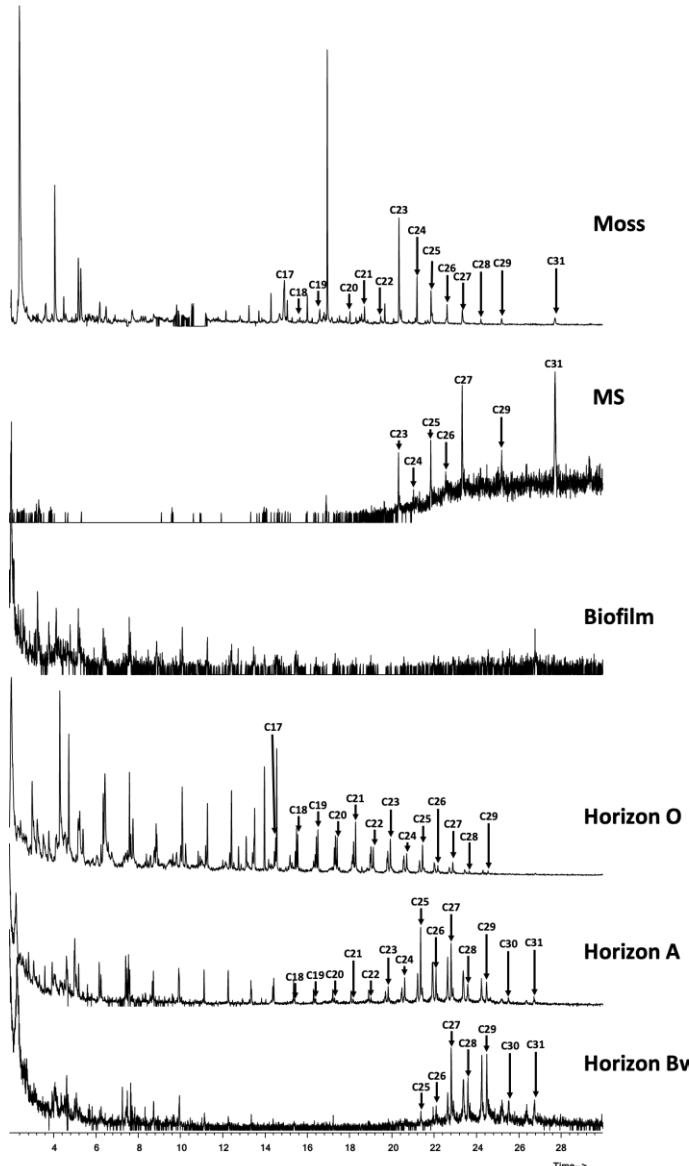
367 In the MS sample, the dominance of odd-chain high-molecular-weight (HMW) *n*-alkanes supported direct organic matter input  
368 from moss. However, the abundance of *n*-tritriacontane ( $C_{33}$ ) and *n*-pentatriacontane ( $C_{35}$ ) *n*-alkanes may also indicate C4  
369 vegetation (Vogts et al., 2009; Feakins et al., 2016) or the adaptation of pre-eruption vegetation to water stress caused by  
370 volcanic ash.

371 In Horizon O, a bimodal *n*-alkane distribution with peaks at  $C_{15}$  and *n*-docosane ( $C_{22}$ ) suggested the presence of organic matter  
372 from soil microorganisms or the degradation of plant biomass by microorganisms over time (Jiménez-Morillo et al., 2016b,  
373 2017). The gradual decline in HMW *n*-alkanes and the absence of a clear odd-over-even pattern indicates microbial degradation  
374 processing of organic matter (De Blas et al., 2013; Jiménez-Morillo et al., 2022; Leal and Jiménez-Morillo et al., 2023). The  
375 higher root density in this layer could also contribute to the observed *n*-alkane pattern.

376 The B<sub>b</sub>iofilm sample was dominated by LMW *n*-alkanes, confirming its microbial origin (Jiménez-Morillo et al., 2017). The  
377 presence of branched alkanes like neophytadiene, 2,6,10-trimethyltridecane, and 2,6,11-trimethyldodecane further supports a  
378 microbial contribution (Palma et al., 2024).

379 In deeper horizons (A and Bw), there is a clearer differentiation between LMW and HMW *n*-alkanes, indicating two carbon  
380 pools from microorganisms (LMW *n*-alkanes) and plant vegetation biomass (HMW *n*-alkanes). The microbial fraction may  
381 stem from lipidic membranes (Miller et al., 2016) or microbial degradation of plant biomass, such as alkyl compounds from  
382 lignocellulose breakdown (Rabbi et al., 2014; Jiménez-Morillo et al., 2022; Miller et al., 2022). The nonspecific aromatic  
383 compounds previously discussed also suggest the lignin breakdown process. However, the most significant differences among  
384 horizons are seen in HMW *n*-alkanes. The Horizon A peaks at *n*-nonacosane ( $C_{29}$ ), indicating tree or shrub vegetation, while  
385 the Horizon Bw peaks at *n*-hentriacontane ( $C_{31}$ ), suggesting herbaceous vegetation (Bull et al., 2000). Therefore, results  
386 indicate a change in vegetation probably due to the alteration of the environmental conditions.

387



389

390 Figure 5: *n*-alkane-2-one (m/z 59) distribution was obtained by direct pyrolysis (Py-GC/MS) of Moss, moss substrate (MS),  
 391 Biofilms and soil horizons (O, A and Bw) samples.

392 The pyrolyzed samples from La Palma, except for the Biofilm sample, revealed a series of *n*-alkane-2-ones (m/z 59 ion  
 393 chromatograms) ranging from C<sub>17</sub> to C<sub>31</sub>, with a general odd-over-even chain-length predominance (Fig. 5). However, each  
 394 sample showed distinct patterns. In the Moss sample, the maximum was at *n*-alkane-2-one C<sub>23</sub>, without a clear parity pattern,

395 though the odd-over-even trend was evident in LMW *n*-alkane-2-ones. This suggests a mixture of lipids from both the moss  
396 and its associated microbiome, as also seen in the *n*-alkanes (Fig. 4).  
397 The MS sample showed a *n*-alkane-2-ones distribution similar to that observed for *n*-alkanes (Fig. 4), being dominated by C<sub>27</sub>  
398 and C<sub>31</sub> molecules, which supports the idea of a direct contribution of organic matter from the Moss.  
399 The soil horizons showed differences in the *n*-alkane-2-one distribution (Fig. 5). In Horizon O, the maximum was at *n*-alkane-  
400 2-one C<sub>21</sub>, while in horizons A and Bw, the maxima were at C<sub>25</sub> and C<sub>27</sub>, respectively. The Horizon O had a range of *n*-alkane-  
401 2-ones from C<sub>17</sub> to C<sub>29</sub>, suggesting more degraded organic matter, possibly due to fine ash deposition affecting organic matter  
402 or microorganisms. In Horizon A, the *n*-alkane-2-one distribution resembled typical soils, with two carbon pools: i) LMW *n*-  
403 alkane-2-ones from microbial activity, and ii) HMW ones from plant-derived organic matter (Jaffé et al., 1996; Kumar et al.,  
404 2020). This aligns with the *n*-alkane distribution (Fig. 4) and overall molecular analysis (Fig. 3). In contrast, the Horizon Bw  
405 contained only HMW *n*-alkane-2-ones (>C<sub>25</sub>), considered biomarkers of vegetation (Kumar et al., 2020; Palma et al., 2024).  
406 This aligns with the isotope carbon signature observed in the soil (Table 1 and Fig. 2) that indicates the influence of microbial  
407 processes at the top layer (Horizon O) and a gradual shift to plant-influenced processes towards the bottom (Horizon Bw). The  
408 absence of LMW *n*-alkane-2-ones in Horizon Bw could be due to concentrations below detection limits, as this horizon had  
409 low TOC (Fig. 1). Environmental factors such as moisture and nutrient availability may affect *n*-alkane-2-one formation by  
410 altering the degradation of *n*-alkanes and *n*-alkanoic acids (Lehtonen and Ketola, 1990; Zhang et al., 2004). Zhang et al. (2004)  
411 identified potential sources of *n*-alkane-2-ones, including: (i) epicuticular waxes from plants; (ii) microbial oxidation of *n*-  
412 alkanes; (iii)  $\beta$ -oxidation and decarboxylation of *n*-alkanoic acids; and (iv) microbial cracking of HMW *n*-alkane-2-ones into  
413 LMW ones. The predominance of LMW *n*-alkane-2-ones in Horizon O further supports an active microbial contribution to  
414 organic matter transformation.

415

416

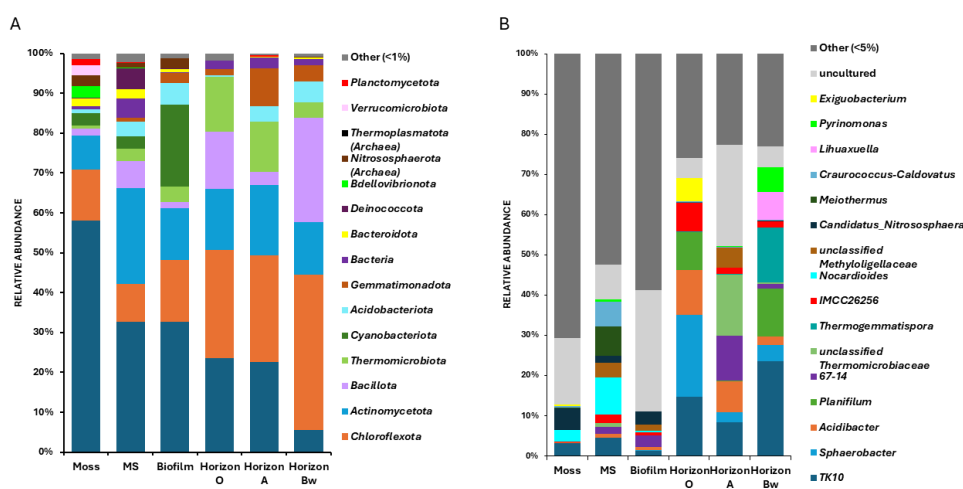
#### 417 3.4 Bacterial community composition

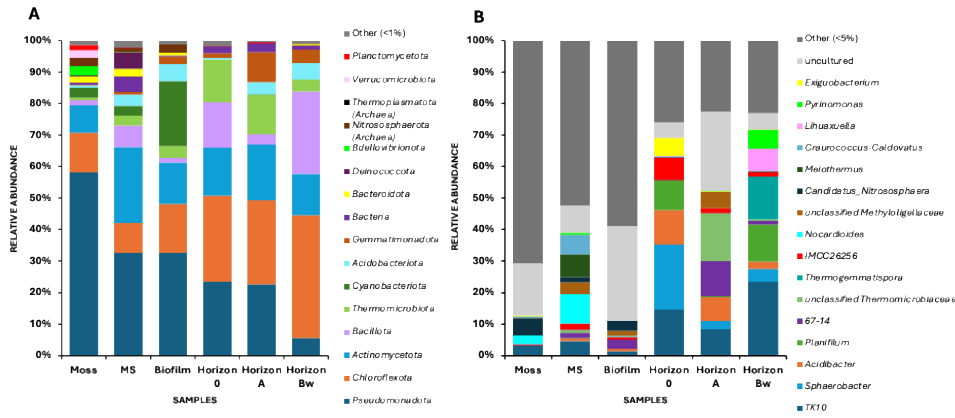
418 A total of 198,129 ASVs (amplicon sequence variants) were analysed from 16S rRNA gene sequencing. The richness and  
419 evenness of microbial communities were estimated using Chao1, Shannon and Simpson indices (Table 2). The Bbiofilm was  
420 the most biodiverse sample, with the highest species richness, and Shannon and Simpson indices of 7.860 and 0.989,  
421 respectively, followed by horizons Bw and A and mossMoss. In contrast, Horizon O showed a lower diversity, with Shannon  
422 and Simpson indices of 4.166 and 0.689, respectively. According to the Chao1 richness estimator, Horizon O and the Bbiofilm  
423 showed the highest predicted microbial richness, indicating that most of the species present in these samples were successfully  
424 detected, with minimal undetected diversity. It is noteworthy that the microbial community in the tephra collected beneath the  
425 moss (MS) reached a substantial diversity and richness within just two years following the deposition of the Tajogaite volcanic  
426 tephra.

428 **Table 2: Alpha diversity 16S of Mmoss, moss substrate (MS), Bbiofilms and soil horizons samples.**

Sample	Shannon	Simpson	chao1	Observed
Moss	6.359	0.973	426.143	426
MS	5.522	0.950	255.500	254
Biofilm	7.860	0.989	832.783	832
Horizon O	4.166	0.689	833.948	829
Horizon A	6.531	0.972	510.315	473
Horizon Bw	7.321	0.972	814.125	812

430 Most of the sequences identified belong to the Bacteria kingdom; however, Archaea, was also found, primarily in the  
 431 mossMoss, biofilm and MS samples, comprising 2.63%, 2.48% and 1.31%, respectively (Fig. 6A). They have been reported  
 432 as early colonizers in samples from the volcanic island *Hunga Tonga Hunga Ha'apai*, in the Kingdom of Tonga (Fujimura et  
 433 al., 2016; Dragone et al., 2023). Archaea are known for their ability to inhabit extreme environments and play critical roles in  
 434 biogeochemical cycles (Offre et al., 2013; Martínez-Espinosa, 2020). The main archaeal class detected in these samples was  
 435 *Nitrososphaeria*, belonging to the phylum *Nitrosphaerota*, which plays a key role in the nitrogen cycle by transforming  
 436 ammonia into nitrite, thereby contributing to the nitrogen availability in the soil. This process indirectly supports plant nutrition  
 437 (Leininger et al., 2006; Lehtovirta-Morley et al., 2024) and influences the distribution of N concentration described in the  
 438 Biofilm and MS samples. The presence of N in these samples infers that the identified genus *Nitrososphaeria* is oxidizing the  
 439 ammonium to nitrite, which requires the presence of oxygen. This might explain the presence of this archaeathese archaea only  
 440 in the mMoss, MS and Biofilm samples, which are in contact with the atmosphere.





442

Figure 6: Relative abundances of microbial phyla (A) and genera (B) across different samples collected from moss, moss substrate (MS), Biofilm, and soil horizons (O, A and Bw) samples.

445

The bacterial phylum *Pseudomonadota* was found in all samples, with relative abundances decreasing with depth, ranging from 58.1% (mMoss) to 5.6% (horizon Bw). Members of this phylum included *Acidibacter*, the *Craurococcus-Caldovatus* bacteria group, and the *Methyloligellaceae* family (Fig. 6B). The acidophilic, ferric iron-reducing, heterotrophic bacterium *Acidibacter*, previously isolated from the Guadiana pit lake, currently has only one described species (Falagán and Johnson, 2014). This bacterium was found in all three horizons, although its abundance decreased with depth, indicating its adaptation to metabolize fresh organic matter, which is more abundant in the Horizon O. The *Caldovatus* genus, a thermophilic bacterium, was found in the MS sample (6.29%). This genus includes only two described species, *C. aquaticus* and *C. sediminis* (Habib et al., 2017; Hu et al., 2022). The *Methyloligellaceae* family is characterised by its ability to use methane as a carbon and energy source, playing a key role in the carbon cycle (Bryukhanov et al., 2024), dominating the Horizon A, MS and Biofilm samples.

Other bacterial genera identified greater than 1% of relative abundance were *Aureimonas*, *Bosea*, *Hyphomonas*, *Legionella*, *Methylorubrum* and *Nordella* in the Mmoss sample; *Candidatus Halysiosphaera*, *Limnobacter*, and *Chthonobacter* in the MS; *Dongia* in the Biofilm; and *Bauldia* in both the Biofilm and Horizon A, and *Brevundimonas* in both the mMoss and MS samples. Notably, the genus *Bosea*, detected in the mMoss sample, is known for its ability to obtain energy through the oxidation of reduced sulfur compounds, a process highly relevant in volcanic environments where sulfur-rich fumaroles, such as those produced during the Tajogaite eruption, have been documented (Martínez-Martínez et al., 2023). Furthermore, this metabolic activity relies on the availability of organic carbon, which was confirmed in all samples through EA/IRMS and Py-GC/MS analyses, highlighting the active coupling between volcanic sulfur emissions and early microbial colonization of the tephra substrate.

465 The phylum *Chloroflexota* was also present in all samples and was particularly abundant in the O, A and Bw horizons, with  
466 relative abundances of 27.23%, 26.77% and 38.92%, respectively. The most abundant members of this phylum were TK10,  
467 S085 and KD4-96, present in all samples along with the thermophilic bacteria *Thermogemmatispora* and *Litorilinea*, found  
468 predominantly in horizon Bw and the *B*biofilm, respectively. Species of *Thermogemmatispora* are involved in carbon  
469 monoxide oxidation in geothermal environments (King and King, 2014). The *Candidatus Chloroploca*, found in the *mMoss*,  
470 is capable of using sulfide oxidation as an electron donor (Gorlenko et al., 2014).

471 The *Actinomycetota* was the most abundant phylum in the MS sample, with the following genera being particularly prominent:  
472 *Nocardioides* (9.33%), IMCC26256 (2.02%), 67-14 (1.64%), *Conexibacter* (1.23%) and *Gatella* (1.01%). In the *B*biofilm, the  
473 *Micronomospora*, *Actinophytocola*, and 67-14 genera were the most abundant, with a relative abundance of 4.16%, 1.81%,  
474 and 2.94%, respectively. In the soil horizons, thermophilic bacteria such as *Thermasporomyces* and *Thermopolyspora* (Horizon  
475 O) and *Thermoleophilum* (dominant in the Horizon Bw) were prevalent. Species of the *Thermopolyspora* genus are capable of  
476 degrading lignocellulosic compounds (Yang et al., 2022), which aligns with the detection of lignin exclusively in the Horizon  
477 O sample by Py-GC/MS. In contrast, members of the genus *Thermoleophilum* can grow exclusively on C<sub>12</sub>–C<sub>19</sub> *n*-alkanes,  
478 cyclohexane, cycloheptane, C<sub>12</sub>–C<sub>18</sub> alcohols and C<sub>13</sub>–C<sub>19</sub> ketones (Yakimov et al., 2003), all of which were identified in the  
479 soil samples through Py-GC/MS (Table S2).

480 The *Bacillota* was a dominant phylum in Horizons Bw (26.29%) and *O* (14.28%), as well as in the MS sample (6.90%). The  
481 most abundant genera within this phylum in the soil horizon samples were *Brockia*, *Thermaerobacter*, *Thermobacillus*, and  
482 *Lihuaxuella* (dominant in the Horizon Bw). The *Limnochorda* was found primarily in all three horizons, while *Planifilum*,  
483 dominant in Horizons *O* and Bw, plays a key role in the degradation of organic matter and harbors potential antibiotic-  
484 resistance genes (Tseng et al., 2024). This genus was also found in the basaltic subsurface of young volcanic islands in Iceland  
485 (Bergsten et al., 2022). Non-thermophilic genera of the *Bacillota* phylum, such as *Exiguobacterium* and *Bacillus*, were also  
486 identified in all three sample types.

487 The *Thermomicrobiota* phylum was present in all samples, particularly in horizons *O* (13.63%) and A (12.53%), mainly  
488 represented by the *Sphaerobacter* genus, which was found in the three soil horizons, with particularly high dominance in  
489 Horizon *O* (20.51%). This bacterium was originally isolated from thermophilically treated sludge, and proteogenomic  
490 analysis indicated that it contains numerous aromatic degradation pathways, such as those involved in lignin degradation  
491 (D'haeseleer et al., 2013), suggesting its role in the breakdown of complex organic matter. Notably, lignin was detected in the  
492 Horizon *O*-sample (Fig. 3), while aromatic compounds have been detected in all samples (Fig. 3).

493 The hyperthermophilic family *Thermomicrobiaceae* was also found, predominantly in horizon A (15.11%), represented by the  
494 67-14 bacterium.

495 The *Cyanobacteriota* phylum was mainly found in the *B*biofilm (20.64%), MS (3.07%), and *mMoss* (3.04%) samples.  
496 Members of this phylum play a crucial role as nitrogen fixers and contribute significantly to the primary production of organic

497 compounds (Rippin et al., 2018), as represented by genera such as *Arthronema* and *Nodosilinea*. This is consistent with the  
498 detection of nitrogen in the B<sub>b</sub>iofilm, MS, and M<sub>m</sub>oss samples, and supported by isotope ratios that predicted the presence of  
499 photosynthetic microorganisms. *Arthronema* is a filamentous cyanobacterium highly adaptive, typical of extreme desert  
500 environments, where it contributes to the nutritional chain and soil formation. Additionally, it exhibits antitumor and  
501 antioxidant properties and produces phycobiliproteins (Iliev and Andreeva, 2006; Chanева et al., 2007; Gardeva et al., 2014;  
502 Petrova et al., 2020). Markers of proteins (peptides) were detected by Py-GC/MS in all samples, except MS. Although this  
503 technique cannot identify specific proteins, the presence of phycobiliproteins cannot be ruled out.

504 Other phyla identified in these samples included *Acidobacteriota*, mainly found in the B<sub>b</sub>iofilm, MS and the A and Bw  
505 horizons; *Gemmamimonadota*, predominantly present in the B<sub>b</sub>iofilm and soil horizon samples; and *Deinococcota* and  
506 *Bacteroidota*, primarily in the MS sample, represented by *Meiothermus* and *Persicitalaea*. The *Deinococcota* phylum is known  
507 as one of the most extremophilic phyla of bacteria, due to its resistance to extreme stressors such as oxidation, radiation,  
508 desiccation, and high temperature (Vilhelmsen et al., 2023).

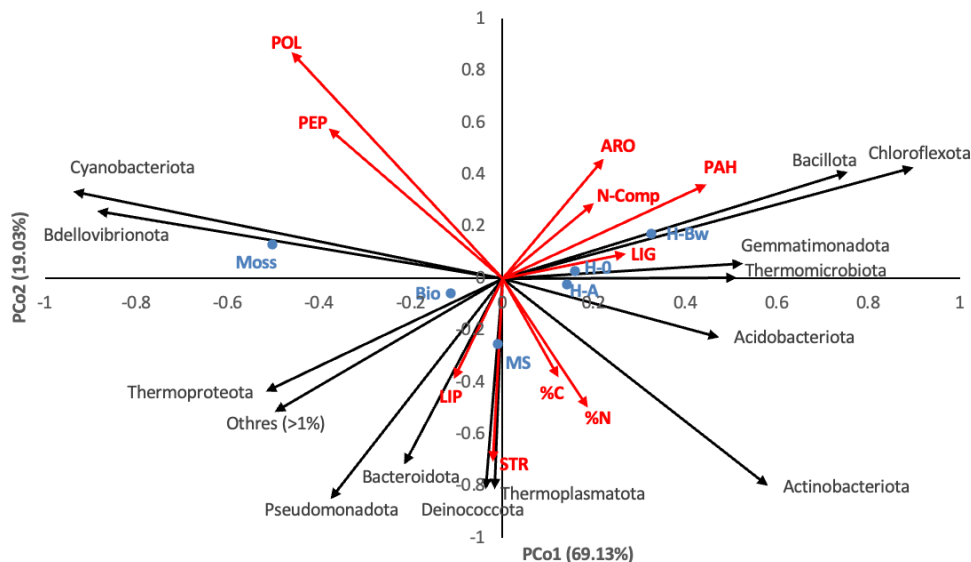
509 In general, the sampling area exhibited a significant presence of thermophilic bacteria, particularly in Horizons O and Bw, and  
510 in the B<sub>b</sub>iofilm. This abundance is likely related to the proximity of steam-emitting fumaroles near the sampling site. These  
511 thermophilic microorganisms, which thrive at elevated temperatures, are highly adapted to the geothermal conditions generated  
512 by the fumaroles. Thermophilic genera such as *Thermasporomyces*, *Thermopolyspora*, *Thermobacillus*, *Planifium* and  
513 *Pyrinomonas*, were observed in the soil horizons. Notably, the only described species of the genus *Pyrinomonas*, *Pyrinomonas*  
514 *methylaliphatogenes*, was originally isolated from geothermally heated soils associated with fumaroles (Crowe et al., 2014).  
515 Members of these genera are recognized for their ability to degrade complex organic materials, such as lignocellulose (Yang  
516 et al., 2022), detected in these soil samples, and for their active role in the degradation of organic matter (Tseng et al., 2024).  
517 This enzymatic capability is particularly beneficial in volcanic soils, where organic matter turnover is critical for early soil  
518 development and nutrient cycling. The dominance of *Thermoleophilum* in the Horizon Bw highlights its ecological role in  
519 metabolizing hydrocarbons, such as PAHs, present in all the soil samples analysed. The hyperthermophilic family  
520 *Thermomicrobiaceae*, predominantly found in Horizon A, and the genus *Sphaerobacter*, highly abundant in the Horizon O, as  
521 well as the thermophilic bacteria *Thermogemmatispora* and *Litorilinea*, predominantly in the deeper soil horizons and the  
522 B<sub>b</sub>iofilm, further underline the influence of geothermal activity on microbial composition.

523 The presence of thermophiles across all collected samples, along with their co-occurrence with non-thermophilic genera,  
524 suggests an ecological adaptation of the microbial community to thermal disturbances associated with volcanic activity and  
525 fumarolic emissions. Furthermore, the relatively lower abundance of thermophiles in horizon A compared to horizons O and Bw  
526 suggests that thermal events occurred more frequently or with great intensity during the formation of horizons O and Bw.  
527 The adaptation of thermophiles to high temperatures enables them to dominate during periods of elevated temperatures (e.g.,  
528 in the presence of fumaroles), while mesophilic counterparts persist and thrive in cooler periods. Temperature and humidity

529 were continuously monitored at the sampling site using a HOBO sensor over one year. During this period, temperatures  
 530 generally fluctuated between 20°C and 30°C, with the highest temperature (51.33°C) recorded on August 12 and the lowest  
 531 (13.76°C) recorded on February 24 (Fig. S1B). The highest temperatures always coincided with the periods of lowest recorded  
 532 humidity.

533

534 **3.5 Linkages between biogeochemical data and microbial community composition**



535  
 536 **Figure 7. Combined principal coordinates analysis (PCoA) of the samples (blue labels) showing the projected loading**  
 537 **weights of geochemical variables (red labels) and the most abundant phyla (black labels).**

538  
 539 To synthesize the coupled patterns observed in the molecular (Py-GC/MS), elemental (%C and %N), and 16S rRNA datasets,  
 540 we explored the ordination space defined by the PCoA biplot (Fig. 7). The first two axes captured over 85% of the multivariate  
 541 structure (PCo1 = 69.13%; PCo2 = 19.03%), revealing a dominant compositional gradient that separates the surface  
 542 colonization system (Mmoss-Bbiofilm-moss substrate) from the mineral soil horizons and, within the latter, differentiates the  
 543 deeper horizon (H-Bw) from the upper layers (H-0 and H-A). PCo1 (69.13%) represents a major change from surface-  
 544 associated, phototrophy-linked communities and labile biopolymers to soil-horizon assemblages associated with more  
 545 processed and thermally-influenced organic pools. On the negative side of PCo1, the Moss sample plots together with vectors  
 546 for *Cyanobacteriota* and *Bdellovibrionota*, consistent with a surface microbiome shaped by primary production and early  
 547 successional colonizers. *Cyanobacteriota* are most prominent in the Bbiofilm and are also present in Moss and MS, supporting  
 548 a role for photosynthetic microorganisms as early sources of organic inputs and nitrogen to the developing system (Rippin et

**Con formato:** Fuente: Negrita

**Con formato:** Fuente: Cursiva

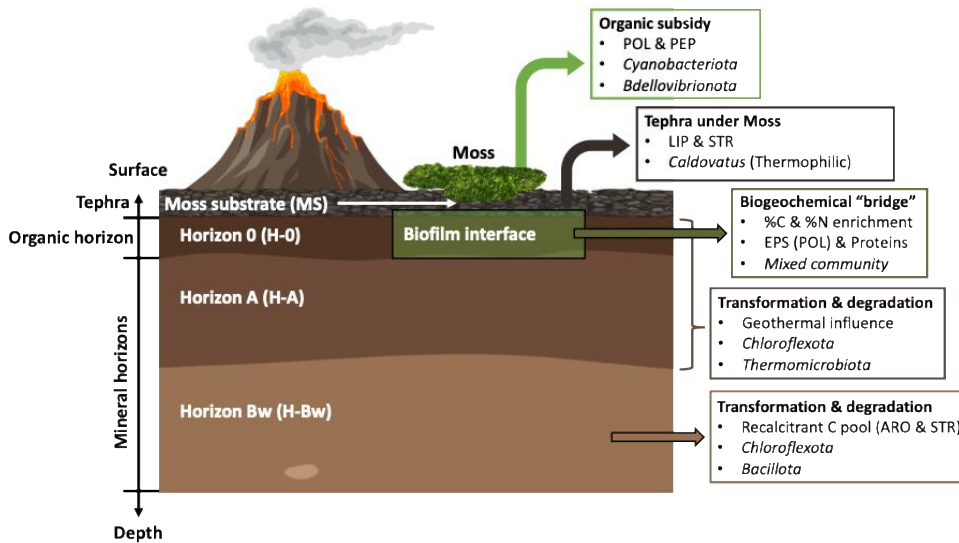
**Con formato:** Fuente: Cursiva

**Con formato:** Fuente: Cursiva

549 al., 2018). In the same direction, the biplot loads polysaccharides (POL) and peptides (PEP) toward positive PCo2 but  
550 negative/near-zero PCo1, matching the expectation that extracellular polymeric substances and proteinaceous biomarkers  
551 contribute strongly to surface/interface organic matter (Palma et al., 2024). This interpretation is aligned with the biofilm  
552 chemistry, since the molecular composition of Bbiofilm is characterized by abundant lipids and aromatics but also a substantial  
553 polysaccharide and peptide fraction (Fig. 3), together with high C and N contents (Table 1). Conversely, the positive side of  
554 PCo1 is driven by soil-horizon taxa and organic families that indicate stronger transformation and/or thermal overprinting. The  
555 deepest horizon (H-Bw) is displaced toward the vectors of *Chloroflexota* and *Bacillota*, two phyla reported as dominant in the  
556 soil horizons (with *Chloroflexota* especially abundant in O, A and Bw, Fig. 6). This association is coherent with the ecological  
557 roles, since thermophilic and thermotolerant groups in these horizons are linked to degradation of complex organic substrates  
558 and hydrocarbons under geothermal influence near fumarolic activity (King and King, 2014). The same positive-PCo1 space  
559 is also aligned with aromatic compounds (ARO), nitrogen-containing compounds (N-Comp) and PAHs, consistent with the  
560 Py-GC/MS evidence that condensed aromatics/PAHs are particularly enhanced in the upper mineral horizon (A), reflecting  
561 pyrogenic inputs and/or strong thermal processing (Fig. 3). Importantly, several of the taxa discussed in the paper (e.g.,  
562 *Thermomicrobiota* representatives such as *Sphaerobacter*) are known to encode aromatic degradation pathways, providing a  
563 mechanistic link between the enrichment in aromatic/PAH-like pools and the microbial potential for their turnover (D'haeseleer  
564 et al., 2013). PCo2 (19.03%) separates biopolymer-rich signatures from lipid/sterane and bulk-elemental signals, helping to  
565 distinguish the interface substrates from the more recalcitrant or source-specific pools. Positive PCo2 is dominated by POL  
566 and PEP, while negative PCo2 loads toward lipids (LIP) and steranes (STR), together with the elemental %C and %N vectors.  
567 In practice, this axis helps explain why Moss (and, to a lesser extent, the biofilm/interface samples) align with  
568 carbohydrate/protein-like inputs typical of fresh biomass and extracellular matrices. In contrast, the moss substrate (MS) shifts  
569 downward along PCo2, consistent with the strong plant-wax/lipid imprint described for MS (odd-dominated high-molecular-  
570 weight  $\mu$ -alkanes indicative of direct plant inputs; Fig. 4). Meanwhile, the sterane signal, preferentially preserved/accumulated  
571 in deeper horizons due to the stability of plant/fungal sterols and related compounds, supports the interpretation that part of  
572 the vertical separation reflects increasing preservation of recalcitrant biomarkers with depth.  
573 The integrated PCoA supports a coherent conceptual model (Fig. 8) for this newly formed tephra–soil system: (i) moss  
574 establishment initiates a surface organic subsidy (biopolymers and labile inputs) and introduces/maintains phototrophy-linked  
575 taxa; (ii) at the interface, biofilms act as a biochemical and ecological “bridge,” concentrating C and N and sustaining a mixed  
576 community consistent with rapid microbial assembly, and (iii) in the mineral horizons, particularly under geothermal influence,  
577 microbial communities change toward phyla and thermophilic lineages associated with the transformation of lignocellulosic  
578 and hydrocarbon pools, matching the observed enrichment in aromatic and PAH-like compounds and the depth-dependent  
579 preservation of stable biomarkers.

Con formato: Fuente: Cursiva

581



582

583 **Figure 8. Integrated conceptual model of the tephra–soil system colonized by moss after volcanic deposition.**584 **4 Conclusions**

585 This study demonstrates that the moss colonizing the upper layer of the tephra deposits releases organic compounds that serve  
 586 as carbon sources for microorganisms, facilitating rapid microbial colonization of the inert volcanic substrate within two years  
 587 after the Tajogaite eruption. This eruption produced a complex tephra blanket exceeding 50 cm in thickness, composed of  
 588 lapilli and fine ash, which accumulated over the pre-existing soil (Horizon O).

589 Our analyses reveal that Horizon  $\text{O}_{\Theta}$  exhibits a distinctive hydrocarbon signature, indicative of both high-temperature thermal  
 590 processes and active microbial transformation of organic matter. In contrast, the deeper soil layers (Horizons A and Bw) display  
 591 alkane patterns characteristic of plant-derived organic matter inputs. Furthermore,  $\delta^{13}\text{C}$  isotopic data strongly suggest intense  
 592 microbial processing of organic carbon in Horizon  $\text{O}_{\Theta}$ , reinforcing the hypothesis that microbial activity significantly  
 593 contributes to the formation of hydrocarbons in this horizon.

594 Importantly, microbial sequencing revealed the presence of taxa capable of hydrocarbon metabolism, including the family  
 595 *Methyloligellaceae*, supporting the hypothesis that some of the detected polycyclic aromatic hydrocarbons (PAHs) could be of  
 596 biogenic origin.

597 In addition, our results indicate that the deposition of fresh tephra materials from the Tajogaite Volcano has the potential to  
 598 alter soil organic matter (SOM) dynamics, favouring the accumulation of labile organic compounds and reducing the  
 599 abundance of recalcitrant components such as lignin, which are typically more resistant to degradation.

Con formato: Fuente: Negrita

501 The dominance of thermophilic bacteria, particularly in Horizons 0O and Bw, highlights their key ecological role in the  
502 breakdown of recalcitrant organic matter, the facilitation of nitrogen and carbon cycling, and the stabilization of the evolving  
503 soil structure. Their metabolic versatility, including the ability to degrade lignin-derived compounds and synthesize  
504 hydrocarbons, positions thermophiles as critical drivers in the early formation of andisols and the recovery of soils disturbed  
505 by volcanic activity.

606 Finally, the persistent presence of thermophilic microorganisms across the studied profile reflects the influence of volcanic  
607 and fumarolic activity in shaping the microbial community structure in the post-eruptive landscape of the Tajogaite Volcano.

608 Given the recurrent volcanic activity on La Palma Island, particularly along the Cumbre Vieja Volcanic Ridge, thermophilic  
609 communities are likely an enduring and essential component of soil ecosystem dynamics in this region.

**Con formato:** Fuente: Cursiva

610

#### 611 **Author contributions**

612 The manuscript was written through the contributions of all authors. All authors have approved the final version of the  
613 manuscript. S.G-P: data curation, formal analysis, methodology, visualization, writing—original draft. A.G.A.: data curation,  
614 formal analysis, methodology, writing—original draft. P.N-J.: methodology, validation, writing—original draft. J.M.-S.:  
615 methodology, validation, writing—review and editing. J.M-M.: methodology, validation, writing—review and editing. B.M-H.:  
616 methodology, writing—review and editing. J.V.: methodology, validation, writing—review and editing. N.T.J.-M.: data curation,  
617 formal analysis, methodology, visualization, validation, writing—original draft, writing—review and editing. A.Z.M.: data  
618 curation, formal analysis, methodology, validation, visualization, supervision, funding acquisition, writing—original draft,  
619 writing—review and editing.

620

#### 621 **Competing interests**

622 The authors declare that they have no conflict of interest.

623

#### 624 **Acknowledgements**

625 This work received support from the Spanish Ministry of Science, Innovation and Universities (MICIU) under the research  
626 project HIRES-SOM (ref. TED2021-130683B-C21/C22) funded by MCIN/AEI/10.13039/501100011033 and the European  
627 Union “NextGenerationEU”/PRTR. The research project MICROLAVA (ref. PROYEXCEL\_00185) funded by Junta de  
628 Andalucía is also acknowledged. N.T. Jiménez-Morillo acknowledges the “Ramón y Cajal” contract (ref. RYC2021-031253-  
629 I) funded by MCIN/AEI/10.13039/501100011033 and the European Union “NextGenerationEU”/PRTR. A. Gómez-Arias  
630 acknowledges the “Juan de la Cierva” contract (ref. JDC2022-049199-I). The authors are grateful to José Heriberto López,  
631 forest officer at the Caldera de Taburiente National Park (La Palma, Spain) for providing logistical support during the sampling  
632 campaign.

634 **Financial support**636 **References**

637 Ågren, G. I., Bosatta, E., and Balesdent, J.: Isotope discrimination during decomposition of organic matter: A theoretical  
638 analysis, *Soil Sci. Soc. Am. J.*, 60, 1121–1126, <https://doi.org/10.2136/sssaj1996.03615995006000040023x>, 1996.

639 Allaguvatova, R. Z., Nikulin, A. Y., Nikulin, V. Y., Bagmet, V. B., and Gaysina, L. A.: Study of biodiversity of algae and  
640 cyanobacteria of Mutnovsky and Gorely volcanoes soils (Kamchatka Peninsula) using a polyphasic approach, *Diversity*, 14,  
641 375, <https://doi.org/10.3390/d14050375>, 2022.

642 Arias, M. E., González-Pérez, J. A., González-Vila, F. J., and Ball, A. S.: Soil health—a new challenge for microbiologists  
643 and chemists, *Int. Microbiol.*, 8, 13–21, 2005.

644 Arnalds, O.: The influence of volcanic tephra (ash) on ecosystems, in: *Advances in Agronomy*, by Sparks, D. L., Academic  
645 Press 121, 331–380, <https://doi.org/10.1016/B978-0-12-407685-3.00006-2>, 2013.

646 Aznar, J. M., González-Pérez, J. A., Badía, D., and Martí, C.: At what depth are the properties of a gypseous forest topsoil  
647 affected by burning? *Land. Degrad. Dev.*, 27, 1344–1353, <https://doi.org/10.1002/lrd.2258>, 2016.

648 Bergsten, P., Vannier, P., Frion, J., Mougeolle, A., and Marteinsson, V. P.: Culturable bacterial diversity from the basaltic  
649 subsurface of the young volcanic island of Surtsey, Iceland, *Microorganisms*, 10, 1177,  
650 <https://doi.org/10.3390/microorganisms10061177>, 2022.

651 Biass, S., Reyes-Hardy, M. P., Gregg, C., Di Maio, L.S., Dominguez, L., Frischknecht, C., Bonadonna, C., and Perez, N.: The  
652 spatiotemporal evolution of compound impacts from lava flow and tephra fallout on buildings: lessons from the 2021 Tajogaite  
653 eruption (La Palma, Spain). *B. Volcanol.*, 86, 10, <https://doi.org/10.1007/s00445-023-01700-w>, 2024.

654 Billings, S. A. and Richter, D. D.: Changes in stable isotopic signatures of soil nitrogen and carbon during 40 years of forest  
655 development, *Oecologia*, 148, 325–333, <https://doi.org/10.1007/s00442-006-0366-7>, 2006.

656 Birnbaum, J., Lev, E., Hernandez, P. A., Barrancos, J., Padilla, G. D., Asensio-Ramos, M., Calvo, D., Rodríguez, F., Pérez, N.  
657 M., D'Auria, L., and Calvari, S.: Temporal variability of explosive activity at Tajogaite volcano, Cumbre Vieja (Canary  
658 Islands), 2021 eruption from ground-based infrared photography and videography, *Front. Earth Sci.*, 11,  
659 <https://doi.org/10.3389/feart.2023.1193436>, 2023.

660 de Blas, E., Almendros, G., and Sanz, J.: Molecular characterization of lipid fractions from extremely water-repellent pine and  
661 eucalyptus forest soils, *Geoderma*, 206, 75–84, <https://doi.org/10.1016/j.geoderma.2013.04.027>, 2013.

662 Bolyen, E., Rideout, J. R., Dillon, M. R., Bokulich, N. A., Abnet, C. C., Al-Ghalith, G. A., Alexander, H., Alm, E. J.,  
663 Arumugam, M., Asnicar, F., Bai, Y., Bisanz, J. E., Bittinger, K., Brejnrod, A., Brislawn, C. J., Brown, C. T., Callahan, B. J.,  
664 Caraballo-Rodríguez, A. M., Chase, J., Cope, E. K., Da Silva, R., Diener, C., Dorrestein, P. C., Douglas, G. M., Durall, D. M.,  
665 Duvall, C., Edwardson, C. F., Ernst, M., Estaki, M., Fouquier, J., Gauglitz, J. M., Gibbons, S. M., Gibson, D. L., Gonzalez,  
666 A., Gorlick, K., Guo, J., Hillmann, B., Holmes, S., Holste, H., Huttonhower, C., Huttley, G. A., Janssen, S., Jarmusch, A. K.,  
667 Jiang, L., Kaehler, B. D., Kang, K. B., Keele, C. R., Keim, P., Kelley, S. T., Knights, D., Koester, I., Kosciolak, T., Kreps, J.,  
668 Langille, M. G. I., Lee, J., Ley, R., Liu, Y. X., Loftfield, E., Lozupone, C., Maher, M., Marotz, C., Martin, B. D., McDonald,  
669 D., McIver, L. J., Melnik, A. V., Metcalf, J. L., Morgan, S. C., Morton, J. T., Nairney, A. T., Navas-Molina, J. A., Nothias, L.  
670 F., Orchania, S. B., Pearson, T., Peoples, S. L., Petras, D., Preuss, M. L., Pruesse, E., Rasmussen, L. B., Rivers, A., Robeson,  
671 M. S., Rosenthal, P., Segata, N., Shaffer, M., Shiffner, A., Sinha, R., Song, S. J., Spear, J. R., Swafford, A. D., Thompson, L. R.,  
672 Torres, P. J., Trinh, P., Tripathi, A., Turnbaugh, P. J., Ul-Hasan, S., van der Hooft, J. J. J., Vargas, F., Vázquez-Baeza, Y.,  
673 Vogtmann, E., von Hippel, M., et al.: Reproducible, interactive, scalable and extensible microbiome data science using QIIME  
674 2, *Nat. Biotechnol.* 37, 852–857, <https://doi.org/10.1038/S41587-019-0209-9>, 2019.

675 Bonadonna, C., Pistolesi, M., Biass, S., Voloschina, M., Romero, J., Coppola, D., Folch, A., D'Auria, L., Marrin-Lorenzo, A.,  
676 Dominguez, L., Pastore, C., Reyes Hardy, M. P., and Rodriguez, F.: Physical characterization of long-lasting hybrid eruptions:  
677 The 2021 tajogaite eruption of cumbre vieja (La Palma, Canary Islands). *J. Geophys. Res-Solid Ea.* 127, 11,  
678 <https://doi.org/10.1029/2022JB025302>, 2022.

679 Bonadonna, C., Pistolesi M., Dominguez L., Freret-Lorgeril, V., Rossi, E., Fries, A., Biass, S., Voloschina, M., Lemus, J.,  
680 Romero, J. E., Zanon V., Pastore C., Reyes Hardy M-P., Di Maio LS., Gabellini P., Martin-Lorenzo A., Rodriguez F., and  
681 Perez, N. M.: Tephra sedimentation and grainsize associated with pulsatory activity: the 2021 Tajogaite eruption of Cumbre  
682 Vieja (La Palma, Canary Islands, Spain). *Front. Earth Sci.* 11:1166073, <https://doi.org/10.3389/feart.2023.1166073>, 2023.

683 Bryukhanov, A. L., Sevastyanov, V. S., Kravchishina, M. D., Voropaev, S. A., Dushenko, N. V., Kurakov, A. V., and Fedulova,  
684 V. Y.: Composition of methane cycle microbial communities in the upper layers of bottom sediments of the Kara sea, *Geochem.  
685 Int.*, 62, 609–617, <https://doi.org/10.1134/S0016702924700277>, 2024.

686 Bull, I. D., Nott, C. J., Van Bergen, P. F., Poulton, P. R., and Evershed, R. P.: Organic geochemical studies of soils from the  
687 Rothamsted classical experiments VI. The occurrence and source of organic acids in an experimental grassland soil, *Soil Biol.*  
688 *Biochem.*, 32, 1367–1376, 2000.

689 Cabianca, A., Müller, L., Pawłowski, K., and Dahlin, P.: Changes in the plant  $\beta$ -sitosterol/stigmastanol ratio caused by the plant  
690 parasitic nematode *meloidogyne incognita*, *Plants*, 10, 1–15, <https://doi.org/10.3390/plants10020292>, 2021.

691 Callahan, B. J., McMurdie, P. J., Rosen, M. J., Han, A. W., Johnson, A. J. A., and Holmes, S. P.: DADA2: High-resolution  
692 sample inference from Illumina amplicon data, *Nat. Methods*, 13, 581–583, <https://doi.org/10.1038/nmeth.3869>, 2016.

693 Campeny, M., Menéndez, I., Ibáñez-Insa, J., Rivera-Martínez, J., Yépes, J., Álvarez-Pousa, S., Méndez-Ramos, J., and  
694 Mangas, J.: The ephemeral fumarolic mineralization of the 2021 Tajogaite volcanic eruption (La Palma, Canary Islands,  
695 Spain). *Sci. Rep.*, 13, 6336, <https://doi.org/10.1038/s41598-023-33387-6>, 2023.

696 Capaccioni, B., Martini, M., and Mangani, F.: Light hydrocarbons in hydrothermal and magmatic fumaroles: hints of catalytic  
697 and thermal reactions, *B. Volcanol.*, 56, 593–600, 1995.

698 Carracedo, J.C., Badiola, E.R., Guillou, H., de la Nuez, J., and Pérez-Torrado, F.J.: Geology and volcanology of la Palma and  
699 El Hierro. *Estud. Geol.*, 57, 175–273, 2001.

700 Carracedo, J. C., Troll, V. R., Day, J. M. D., Geiger, H., Aulinás, M., Soler, V., Deegan, F. M., Perez-Torrado, F. J., Gisbert, G.,  
701 Gazel, E., Rodriguez-Gonzalez, A., and Albert, H.: The 2021 eruption of the Cumbre Vieja volcanic ridge on La Palma, Canary  
702 Islands, *Geology Today*, 38, 94–107, <https://doi.org/10.1111/gto.12388>, 2022.

703 Carrell, A. A., Veličković, D., Lawrence, T. J., Bowen, B. P., Louie, K. B., Carper, D. L., Chu, R. K., Mitchell, H. D., Orr, G.,  
704 Markillie, L. M., Jawdy, S. S., Grimwood, J., Shaw, A. J., Schmutz, J., Northen, T. R., Anderton, C. R., Pelletier, D. A., and  
705 Weston, D. J.: Novel metabolic interactions and environmental conditions mediate the boreal peatmoss-cyanobacteria  
706 mutualism, *ISME J.*, 16, 1074–1085, <https://doi.org/10.1038/s41396-021-01136-0>, 2022.

707 Chaneva, G., Furnadzhieva, S., Minkova, K., and Lukavsky, J.: Effect of light and temperature on the cyanobacterium  
708 *Arthronema africanum* - A prospective phycobiliprotein-producing strain, *J. Appl. Phycol.*, 19, 537–544,  
709 <https://doi.org/10.1007/s10811-007-9167-6>, 2007.

710 Chen, J., Zheng, Y., Guo, Y., Li, F., Xu, D., Chao, L., Qu, H., Wang, B., Ma, X., Wang, S., and Bao, Y.: Differences in microbial  
711 communities from Quaternary volcanic soils at different stages of development: Evidence from Late Pleistocene and Holocene  
712 volcanoes, *Catena (Amst)*, 201, <https://doi.org/10.1016/j.catena.2021.105211>, 2021.

713 Craig, H., Wilson, T., Stewart, C., Outes, V., Villarosa, G., and Baxter, P.: Impacts to agriculture and critical infrastructure in  
714 Argentina after ashfall from the 2011 eruption of the Cordon Caulle volcanic complex: An assessment of published damage  
715 and function thresholds, *J. Appl. Volcanol.*, 5, 7, <https://doi.org/10.1186/s13617-016-0046-1>, 2016.

716 Crowe, M. A., Power, J. F., Morgan, X. C., Dunfield, P. F., Lagutin, K., Rijpstra, W. I. C., Rijpstra, I. C., Sinninghe Damste, J.  
717 S., Houghton, K. M., Ryan, J. L. J., and Stott, M. B.: *Pyrinomonas methylaliphaticogenes* gen. nov., sp. nov., a novel group 4  
718 thermophilic member of the phylum Acidobacteria from geothermal soils, *Int. J. Syst. Evol. Micr.*, 64, 220–227,  
719 <https://doi.org/10.1099/ijsm.0.055079-0>, 2014.

720 Das, S. K.: *Bosea*, in: *Bergey's Manual of Systematics of Archaea and Bacteria*, edited by Whitman, W. B., Wiley, J., and Sons,  
721 Ltd., Hoboken, N.J., USA, 1–4, <https://doi.org/10.1002/9781118960608.gbm00801>, 2015.

722 De la Rosa, J. M., Jiménez-Morillo, N. T., González-Pérez, J. A., Almendros, G., Vieira, D., Knicker, H. E., and Keizer, J.:  
723 Mulching-induced preservation of soil organic matter quality in a burnt eucalypt plantation in central Portugal, *J. Environ.*  
724 *Manage.*, 231, 1135–1144, <https://doi.org/10.1016/j.jenvman.2018.10.114>, 2019.

725 De la Rosa, J. M., Pérez-Dalí, S. M., Campos, P., Sánchez-Martín, Á., González-Pérez, J. A., and Miller, A. Z.: Suitability of  
726 volcanic ash, rice husk ash, green compost and biochar as amendments for a Mediterranean alkaline soil, *Agronomy*, 13, 4,  
727 <https://doi.org/10.3390/agronomy13041097>, 2023.

728 Dhabalia Ashok, A., De Vries, S., Darienko, T., Irisarri, I., and De Vries, J.: Evolutionary assembly of the plant terrestrialization  
729 toolkit from protein domains, *P. Roy. Soc. B-Biol. Sci.*, 291, <https://doi.org/10.1098/rspb.2024.0985>, 2024.

730 D'haeseleer, P., Gladden, J. M., Allgaier, M., Chain, P. S. G., Tringe, S. G., Malfatti, S. A., Aldrich, J. T., Nicora, C. D.,  
731 Robinson, E. W., Pasa-Tolić, L., Hugenholtz, P., Simmons, B. A., and Singer, S. W.: Proteogenomic analysis of a thermophilic  
732 bacterial consortium adapted to deconstruct switchgrass, *PLOS One*, 8, <https://doi.org/10.1371/journal.pone.0068465>, 2013.

733 Dragone, N. B., Whittaker, K., Lord, O. M., Burke, E. A., Dufel, H., Hite, E., Miller, F., Page, G., and Slayback, D.: The early  
734 microbial colonizers of a short-lived volcanic island in the Kingdom of Tonga, *mBio*, 14, 1,  
735 <https://doi.org/10.1128/mbio.03313-22>, 2023.

736 Ehleringer, J. R., Buchmann, N., and Flanagan, L. B.: Carbon isotope ratios in belowground carbon cycle processes, *Ecol.*  
737 *Appl.*, 10, 412–422, <https://doi.org/10.2307/2641103>, 2000.

738 Falagán, C. and Johnson, D. B.: *Acidibacter ferrireducens* gen. nov., sp. nov.: an acidophilic ferric iron-reducing  
739 gammaproteobacterium. *Extremophiles*, 18, 1067–1073, <https://doi.org/10.1007/s00792-014-0684-3>, 2014.

740 Feakins, S. J., Peters, T., Wu, M. S., Shenkin, A., Salinas, N., Girardin, C. A. J., Bentley, L. P., Blonder, B., Enquist, B. J.,  
741 Martin, R.E., Asner, G. P., and Malhi, Y.: Production of leaf wax n-alkanes across a tropical forest elevation transect. *Org. Geochem.*, 100, 89-100, <https://doi.org/10.1016/j.orggeochem.2016.07.004>, 2016.

743 Ferrer, N., Marrero-Rodríguez, N., Sanromualdo-Collado, A., Vegas, J., and García-Romero, L.: Early morphodynamics of the  
744 sudden formation of beaches during the 2021 volcanic eruption of La Palma, *Geomorphology*, 436,  
745 <https://doi.org/10.1016/j.geomorph.2023.108779>, 2023.

746 Fraser, C. M. and Chapple, C.: The phenylpropanoid pathway in *Arabidopsis*, *Arabidopsis Book*, 9, e0152,  
747 <https://doi.org/10.1199/tab.0152>, 2011.

748 Fujimura, R., Kim, S. W., Sato, Y., Oshima, K., Hattori, M., Kamijo, T., and Ohta, H.: Unique pioneer microbial communities  
749 exposed to volcanic sulfur dioxide, *Sci. Rep.*, 6, 19687, <https://doi.org/10.1038/srep19687>, 2016.

750 García-Carmona, M., García-Orenes, F., Arcenegui, V., and Mataix-Solera, J.: The recovery of mediterranean soils after post-  
751 fire management: The role of biocrusts and soil microbial communities, *Span. J. Soil Sci.*, 13,  
752 <https://doi.org/10.3389/sjss.2023.11388>, 2023.

753 Gardeva, E. G., Toshkova, R. A., Yossifova, L. S., Minkova, K., Ivanova, N. Y., and Gigova, L. G.: Antitumor activity of C-  
754 phycocyanin from *Arthronema africanum* (Cyanophyceae), *Braz. Arch. Biol. Techn.*, 57, 675-684,  
755 <https://doi.org/10.1590/S1516-89132014005000018>, 2014.

756 Ghezzi, D., Jiménez-Morillo, N. T., Foschi, L., Donini, E., Chiarini, V., De Waele, J., Miller, A. Z., and Cappelletti, M.: The  
757 microbiota characterizing huge carbonatic moonmilk structures and its correlation with preserved organic matter, *Environ.*  
758 *Microbiome*, 19, 25, <https://doi.org/10.1186/s40793-024-00562-9>, 2024.

759 Girona-García, A., Badía-Villas, D., Jiménez-Morillo, N. T., de la Rosa, J. M., and González-Pérez, J. A.: Soil C and N isotope  
760 composition after a centennial Scots pine afforestation in podzols of native European beech forests in NE-Spain, *Catena*  
761 (Amst), 165, 434-441, <https://doi.org/10.1016/j.catena.2018.02.023>, 2018.

762 González-Pérez, J. A., González-Vila, F. J., Almendros, G., and Knicker, H.: The effect of fire on soil organic matter - A review,  
763 *Environ. Int.*, 30, 855-870, <https://doi.org/10.1016/j.envint.2004.02.003>, 2004.

764 González-Pérez, J. A., Almendros, G., De La Rosa, J. M., and González-Vila, F. J.: Appraisal of polycyclic aromatic  
765 hydrocarbons (PAHs) in environmental matrices by analytical pyrolysis (Py-GC/MS), *J. Anal. Appl. Pyrol.*, 109, 1-8,  
766 <https://doi.org/10.1016/j.jaap.2014.07.005>, 2014.

767 González-Pérez, J. A., Jiménez-Morillo, N. T., de la Rosa, J. M., Almendros, G., and González-Vila, F. J.: Compound-specific  
768 stable carbon isotopic signature of carbohydrate pyrolysis products from C3 and C4 plants, *J. Sci. Food. Agric.*, 96, 948-953,  
769 <https://doi.org/10.1002/jsfa.7169>, 2016.

770 Gorlenko, V. M., Bryantseva, I. A., Kalashnikov, A. M., Gaisin, V. A., Sukhacheva, M. V., Gruzdev, D. S., and Kuznetsov, B.  
771 B.: *Candidatus 'Chloroploca asiatica'* gen. nov., sp. nov., a new mesophilic filamentous anoxygenic phototrophic bacterium,  
772 *Microbiology (Russian Federation)*, 83, 838-848, <https://doi.org/10.1134/S002661714060083>, 2014.

773 Guarro, J., Abdullah, S. K., Al-Bader, S. M., Figueras, M. J., and Gené, J.: The genus *Melanocarpus*, *Mycol. Res.*, 100, 75-  
774 78, [https://doi.org/10.1016/S0953-7562\(96\)80103-1](https://doi.org/10.1016/S0953-7562(96)80103-1), 1996.

775 Gutierrez-Patricio, S., Osman, J. R., Luis Gonzalez-Pimentel, J., Jurado, V., Laiz, L., Laínez Concepción, A., Saiz-Jimenez,  
776 C., and Miller, A. Z.: Microbiological exploration of the Cueva del Viento lava tube system in Tenerife, Canary Islands, *Env.*  
777 *Microbiol. Rep.*, 16, e13245, <https://doi.org/10.1111/1758-2229.13245>, 2024.

778 Habib, N., Khan, I. U., Hussain, F., Zhou, E. M., Xiao, M., Ahmed, I., Zhi, X. Y., and Li, W. J.: *Caldovatus sediminis* gen.  
779 nov., sp. nov., a moderately thermophilic bacterium isolated from a hot spring, *Int. J. Syst. Evol. Microbiol.*, 67, 4716-4721,  
780 <https://doi.org/10.1099/ijsem.0.002363>, 2017.

781 Hadland, N., Hamilton, C. W., and Duhamel, S.: Young volcanic terrains are windows into early microbial colonization,  
782 *Commun. Earth Environ.*, 5, 114, <https://doi.org/10.1038/s43247-024-01280-3>, 2024.

783 Hernández, Z., Almendros, G., Carral, P., Álvarez, A., Knicker, H., and Pérez-Trujillo, J. P.: Influence of non-crystalline  
784 minerals in the total amount, resilience and molecular composition of the organic matter in volcanic ash soils (Tenerife Island,  
785 Spain), *Eur. J. Soil Sci.*, 63, 603-615, <https://doi.org/10.1111/j.1365-2389.2012.01497.x>, 2012.

786 Hoernle, K. A. J., Carracedo, J. C., Canary Islands, geology, University of California Press, 2009.

787 Höglberg, P.: Tansley review no. 95 natural abundance in soil-plant systems, *New Phytol.*, 137, 179-203,  
788 <https://doi.org/10.1046/j.1469-8137.1997.00808.x>, 1997.

789 Hu, C. J., Xian, W. D., Lv, Y. Q., Peng, C. X., Shan, R. X., Cheng, Z. C., Lv, Q., Tian, Y., Jiao, J. Y., Tan, S., and Li, W.  
790 J.: *Caldovatus aquaticus* sp. nov., a moderately thermophilic bacterium isolated from hot spring microbial mat. *Int. J. Syst.*  
791 *Evol. Microbiol.*, 72, 5627, <https://doi.org/10.1099/ijsem.0.005627>, 2022.

792 Iliev, I. P. G. D. and Andreeva, R.: Membrane metabolites of *Arthronema africanum* strains from extreme habitats, *Gen. Appl.*  
793 *Plant. Physiology*, 2006, 117-123, 2006.

794 Ingimundardóttir, G. V., Weibull, H., and Cronberg, N.: Bryophyte colonization history of the virgin volcanic Island Surtsey,  
795 Iceland, *Biogeosciences*, 11, 4415–4427, <https://doi.org/10.5194/bg-11-4415-2014>, 2014.

796 Iwasaki, S., Endo, Y., Hatano, R., and Toma, Y.: Factors impacting soil organic carbon pool in different types of Andosols in  
797 Toya, Hokkaido, Japan, *Soil Sci. Plant. Nutr.*, 67, 594–605, <https://doi.org/10.1080/00380768.2021.1959836>, 2021.

798 Jaffé, R., Elismé, T., and Cabrera, A. C.: Organic geochemistry of seasonally flooded rain forest soils: molecular composition  
799 and early diagenesis of lipid components, *Org. Geochem.*, 25, 9–17, 1996.

800 Jiménez-Morillo, N. T., de la Rosa, J. M., Waggoner, D., Almendros, G., González-Vila, F. J., and González-Pérez, J. A.: Fire  
801 effects in the molecular structure of soil organic matter fractions under *Quercus suber* cover, *Catena*, 145, 266–273,  
802 <https://doi.org/10.1016/j.catena.2016.06.022>, 2016a.

803 Jiménez-Morillo, N. T., González-Pérez, J. A., Jordán, A., Zavala, L. M., de la Rosa, J. M., Jiménez-González, M. A., and  
804 González-Vila, F. J.: Organic matter fractions controlling soil water repellency in sandy soils from the Doñana national park  
805 (Southwestern Spain), *Land. Degrad. Dev.*, 27, 1413–1423, <https://doi.org/10.1002/lrd.2314>, 2016b.

806 Jiménez-Morillo, N. T., Spangenberg, J. E., Miller, A. Z., Jordán, A., Zavala, L. M., González-Vila, F. J., and González-Pérez,  
807 J. A.: Wildfire effects on lipid composition and hydrophobicity of bulk soil and soil size fractions under *Quercus suber* cover  
808 (SW-Spain), *Environ. Res.*, 159, 394–405, <https://doi.org/10.1016/j.envres.2017.08.022>, 2017.

809 Jiménez-Morillo, N. T., González-Pérez, J. A., Almendros, G., De la Rosa, J. M., Waggoner, D. C., Jordán, A., Zavala, L. M.,  
810 González-Vila, F. J., and Hatcher, P. G.: Ultra-high resolution mass spectrometry of physical speciation patterns of organic  
811 matter in fire-affected soils, *J. Environ. Manage.*, 225, 139–147, <https://doi.org/10.1016/j.jenvman.2018.07.069>, 2018.

812 Jiménez-Morillo, N. T., Almendros, G., De la Rosa, J. M., Jordán, A., Zavala, L. M., Granged, A. J. P., and González-Pérez, J.  
813 A.: Effect of a wildfire and of post-fire restoration actions in the organic matter structure in soil fractions, *Sci. Total Environ.*,  
814 728, 138715, <https://doi.org/10.1016/j.scitotenv.2020.138715>, 2020a.

815 Jiménez-Morillo, N. T., Almendros, G., González-Vila, F. J., Jordán, A., Zavala, L. M., de la Rosa, J. M., and González-Pérez,  
816 J. A.: Fire effects on C and H isotopic composition in plant biomass and soil: Bulk and particle size fractions, *Sci. Total  
817 Environ.*, 749, 141417, <https://doi.org/10.1016/j.scitotenv.2020.141417>, 2020b.

818 Jiménez-Morillo, N. T., Almendros, G., Miller, A. Z., Hatcher, P. G., and González-Pérez, J. A.: Hydrophobicity of soils  
819 affected by fires: An assessment using molecular markers from ultra-high resolution mass spectrometry, *Sci. Total Environ.*,  
820 817, 152957, <https://doi.org/10.1016/j.scitotenv.2022.152957>, 2022.

821 Katsumi, N., Yonebayashi, K., Fujitake, N., and Okazaki, M.: Relationship between stable carbon and nitrogen isotope ratios  
822 of humic acids extracted from Andisols and non-Andisols, *Catena (Amst)*, 127, 214–221,  
823 <https://doi.org/10.1016/j.catena.2015.01.005>, 2015.

824 Kellner, H., Luis, P., Pecyna, M. J., Barbi, F., Kapturska, D., Kruiger, D., Zak, D. R., Marmeisse, R., Vandenbol, M., and  
825 Hofrichter, M.: Widespread occurrence of expressed fungal secretory peroxidases in forest soils, *PLOS One*, 9, e95557,  
826 <https://doi.org/10.1371/journal.pone.0095557>, 2014.

827 King, C. E. and King, G. M.: Description of *Thermogemmatispora carboxidivorans* sp. nov., a carbon-monoxide-oxidizing  
828 member of the class Ktedonobacteria isolated from a geothermally heated biofilm, and analysis of carbon monoxide oxidation  
829 by members of the class Ktedonobacteria, *Int. J. Syst. Evol. Microbiol.*, 64, 1244–1251, <https://doi.org/10.1099/ijsm.0.059675-0>, 2014.

831 Klavina, L., Springe, G., Nikolajeva, V., Martsinkevich, I., Nakurte, I., Dzabijeva, D., and Steinberga, I.: Molecules chemical  
832 composition analysis, antimicrobial activity and cytotoxicity screening of moss extracts (Moss Phytochemistry), *Molecules*,  
833 20, 17221–17243, <https://doi.org/10.3390/molecules200917221>, 2015.

834 Klegin, C., Ethur, E. M., Bordin, J., and Baia Figueiredo, P. L.: Chemical composition of essential oil from mosses from the  
835 brazilian atlantic forest, *Chem. Biodivers.*, 20, e202300286, <https://doi.org/10.1002/cbdv.202300286>, 2023.

836 Krauss, M., Wilcke, W., Martius, C., Bandeira, A. G., Garcia, M. V. B., Amelung, W.: Atmospheric versus biological sources  
837 of polycyclic aromatic hydrocarbons (PAHs) in a tropical rain forest environment. *Environ. Pollut.*, 135, 143–154,  
838 <https://doi.org/10.1016/j.envpol.2004.09.012>, 2005.

839 Kristan, K. and Rižner, T. L.: Steroid-transforming enzymes in fungi, *J. Steroid. Biochem. Mol. Biol.*, 129, 79–91,  
840 <https://doi.org/10.1016/j.jsbmb.2011.08.012>, 2012.

841 Krüger, N., Finn, D. R., and Don, A.: Soil depth gradients of organic carbon-13 – A review on drivers and processes, *Plant  
842 Soil*, 495, 113–136, <https://doi.org/10.1007/s11104-023-06328-5>, 2024.

843 Kumar, M., Boski, T., González-Vila, F. J., Jiménez-Morillo, N. T., and González-Pérez, J. A.: Characteristics of organic matter  
844 sources from Guadiana Estuary salt marsh sediments (SW Iberian Peninsula), *Cont. Shelf Res.*, 197, 104076,  
845 <https://doi.org/10.1016/j.csr.2020.104076>, 2020.

846 Ladygina, N., Dedyukhina, E. G., and Vainshtein, M. B.: A review on microbial synthesis of hydrocarbons. *Process Biochem.*,  
847 41, 1001–1014, <https://doi.org/10.1016/j.procbio.2005.12.007>, 2006.

848 Leal, O. dos A., Jiménez-Morillo, N. T., González-Pérez, J. A., Knicker, H., de Souza Costa, F., Jiménez-Morillo, P. N., de  
849 Carvalho Júnior, J. A., dos Santos, J. C., and Pinheiro Dick, D.: Soil organic matter molecular composition shifts driven by  
850 forest regrowth or pasture after slash-and-burn of amazon forest, *Int. J. Environ. Res. Public Health*, 20, 3485,  
851 https://doi.org/10.3390/ijerph20043485, 2023.

852 Lehtonen, K. and Ketola, M.: Occurrence of long-chain acyclic methyl ketones in *Sphagnum* and *Carex* peats of various  
853 degrees of humification, *Org. Geochem.*, 15, 275–280, https://doi.org/10.1016/0146-6380(90)90005-K, 1990.

854 Lehtovirta-Morley, L. E., Ge, C., Ross, J., Yao, H., Hazard, C., Gubry-Rangin, C., Prosser, J. I., and Nicol, G. W.: *Nitrosotalea*  
855 *devaniterrae* gen. nov., sp. nov. and *Nitrosotalea sinensis* sp. nov., two acidophilic ammonia oxidising archaea isolated from  
856 acidic soil, and proposal of the new order *Nitrosotaleales* ord. nov. within the class *Nitrosphaeria* of the phylum  
857 *Nitrosphaerota*, *Int. J. Syst. Evol. Microbiol.*, 74, https://doi.org/10.1099/ijsem.0.006387, 2024.

858 Leininger, S., Urich, T., Schloter, M., Schwark, L., Qi, J., Nicol, G. W., Prosser, J. I., Schuster, S. C., and Schleper, C.:  
859 Archaea predominate among ammonia-oxidizing prokaryotes in soils, *Nature*, 442, 806–809,  
860 https://doi.org/10.1038/nature04983, 2006.

861 Longpré, M.-A., Felpeto, A.: Historical volcanism in the Canary Islands; part 1: A review of precursory and eruptive activity,  
862 eruption parameter estimates, and implications for hazard assessment, *J. Volcanol. Geoth. Res.*, 419, 107363,  
863 https://doi.org/10.1016/j.volgeores.2021.107363, 2021.

864 Love, C. R., Arrington, E. C., Gosselin, K. M., Reddy, C. M., Van Mooy, B. A. S., Nelson, R. K., and Valentine, D. L.: Microbial  
865 production and consumption of hydrocarbons in the global ocean. *Nat. Microbiol.* 6, 489–498, https://doi.org/10.1038/s41564-  
866 020-00859-8, 2021.

867 Nanzyo, M., Dahlgren, R. and Shoji, S.: Chemical characteristics of volcanic ash soils. In: Shoji, S., Nanzyo, M. and Dahlgren,  
868 R., edited by *Volcanic Ash Soils—Genesis, Properties and Utilization, Developments in Soil Science*, Elsevier, Amsterdam,  
869 145–188, http://dx.doi.org/10.1016/S0166-2481(08)70267-8, 1993.

870 Makarov, M. I.: The nitrogen isotopic composition in soils and plants: Its use in environmental studies (A Review), *Soil  
871 Chemistry*, 42, 1335–1347, https://doi.org/10.1134/S1064229309120035, 2009.

872 Martínez-Espinosa, R. M.: Microorganisms and their metabolic capabilities in the context of the biogeochemical nitrogen cycle  
873 at extreme environments, *Int. J. Mol. Sci.*, 21, 4228, https://doi.org/10.3390/ijms21124228, 2020.

874 Martínez-Martínez, J., Mediato, J. F., Mata, M. P., Ordóñez, B., del Moral, B., Bellido, E., Pérez-López, R., Rodríguez-Pascua,  
875 M. A., Vegas, J., Lozano Otero, G., Mateos, R. M., Sánchez, N., and Galindo, I.: Early fumarolic minerals from the Tajogaite  
876 volcanic eruption (La Palma, 2021), *J. Volcanol. Geotherm. Res.*, 435, 107771,  
877 https://doi.org/10.1016/j.volgeores.2023.107771, 2023.

878 Matus, F., Rumpel, C., Neculman, R., Panichini, M., and Mora, M. L.: Soil carbon storage and stabilisation in andic soils: A  
879 review, *Catena*, 120, 102–110, https://doi.org/10.1016/j.catena.2014.04.008, 2014.

880 Miller, A. Z., De la Rosa, J. M., Jiménez-Morillo, N. T., Pereira, M. F. C., González-Pérez, J. A., Calaforra, J. M., Saiz-Jimenez,  
881 C.: (2016). Analytical pyrolysis and light stable isotope analyses reveal environmental changes in coralloid speleothems from  
882 Easter Island (Chile). *J. Chromatogr. A*, 1461, 144–152, https://doi.org/10.1016/j.chroma.2016.07.038, 2016.

883 Miller, A. Z., De la Rosa, J. M., Jiménez-Morillo, N. T., Pereira, M. F. C., Gonzalez-Perez, J. A., Knicker, H., and Saiz-Jimenez,  
884 C.: Impact of wildfires on subsurface volcanic environments: New insights into speleothem chemistry, *Science of the Total  
885 Environment*, 698, https://doi.org/10.1016/j.scitotenv.2019.134321, 2020.

886 Miller, A. Z., Jiménez-Morillo, N. T., Coutinho, M. L., Gazquez, F., Palma, V., Sauro, F., Pereira, M. F. C., Rull, F., Toulkeridis,  
887 T., Caldeira, A. T., Forti, P., and Calaforra, J. M.: Organic geochemistry and mineralogy suggest anthropogenic impact in  
888 speleothem chemistry from volcanic show caves of the Galapagos, *iScience*, 25, 104556,  
889 https://doi.org/10.1016/j.isci.2022.104556, 2022.

890 Mohapatra, B. and Phale, P. S.: Microbial degradation of naphthalene and substituted naphthalenes: Metabolic diversity and  
891 genomic insight for bioremediation, *Front. Bioeng. Biotechnol.*, 9, https://doi.org/10.3389/fbioe.2021.602445, 2021.

892 Muneer, M. A., Huang, X., Hou, W., Zhang, Y., Cai, Y., Munir, M. Z., Wu, L., and Zheng, C.: Response of fungal diversity,  
893 community composition, and functions to nutrients management in red soil, *J. Fungi*, 7, 554,  
894 https://doi.org/10.3390/jof7070554, 2021.

895 Muñoz, G., Orlando, J., and Zuñiga-Feest, A.: Plants colonizing volcanic deposits: root adaptations and effects on rhizosphere  
896 microorganisms, *Plant Soil*, 461, 265–279, https://doi.org/10.1007/s11104-020-04783-y, 2021.

897 Musat, F., Galushko, A., Jacob, J., Widdel, F., Kube, M., Reinhardt, R., Wilkes, H., Schink, B., and Rabus, R.: Anaerobic  
898 degradation of naphthalene and 2-methylnaphthalene by strains of marine sulfate-reducing bacteria, *Environ. Microbiol.*, 11,  
899 209–219, https://doi.org/10.1111/j.1462-2920.2008.01756.x, 2009.

900 Nierop, K. G. J. and Buurman, P.: Thermally assisted hydrolysis and methylation of organic matter in two allophanic volcanic  
901 ash soils from the Azores Islands, in: *Soils of Volcanic Regions in Europe*, edited by: Arnalds, O., óskarsson, H., Bartolini, F.,

902 Buurman, P., Stoops, G., García-Rodeja, E. Springer, Berlin, Heidelberg, [https://doi.org/10.1007/978-3-540-48711-1\\_30](https://doi.org/10.1007/978-3-540-48711-1_30),  
903 2007.

904 Offre, P., Spang, A., and Schleper, C.: Archaea in biogeochemical cycles, *Annu. Rev. Microbiol.*, 67, 437–457,  
905 <https://doi.org/10.1146/annurev-micro-092412-155614>, 2013.

906 Palma, V., De la Rosa, J. M., Onac, B. P., Sauro, F., Martínez-Frías, J., Caldeira, A. T., González-Pérez, J. A., Jiménez-Morillo,  
907 N. T., and Miller, A. Z.: Decoding organic compounds in lava tube sulfates to understand potential biomarkers in the Martian  
908 subsurface, *Commun. Earth Environ.*, 5, 530, <https://doi.org/10.1038/s43247-024-01673-4>, 2024.

909 Peng, X., Tamura, K., Asano, M., Takano, A., Kawagoe, M., and Kamijo, T.: Changes in soil physical and chemical properties  
910 during vegetation succession on miyake-jima island, *Forests*, 12, 1435, <https://doi.org/10.3390/f12111435>, 2021.

911 Petkova, Z., Teneva, O., Antova, G., Angelova-Romova, M., Gecheva, G., and Dimitrova-Dyulgerova, I.: Chemical  
912 composition, lipid-soluble bioactive compounds and potential health benefits of the moss *Hypnum cupressiforme* Hedw, *Plants*,  
913 12, 4190, <https://doi.org/10.3390/plants12244190>, 2023.

914 Petrova, D. H., Yocheva, L., and Petrova, M.: Antimicrobial and antioxidant activities of microalgal extracts, *Oxid. Commun.*,  
915 43, 103–116, <https://doi.org/10.13140/RG.2.2.20509.84963>, 2020.

916 Quast, C., Pruesse, E., Yilmaz, P., Gerken, J., Schweer, T., Yarza, P., Peplies, J., and Glöckner, F. O.: The SILVA ribosomal  
917 RNA gene database project: Improved data processing and web-based tools, *Nucleic Acids Res.*, 41, D590-D596,  
918 <https://doi.org/10.1093/nar/gks1219>, 2013.

919 Rabbi, S. M. F., Wilson, B. R., Lockwood, P. V., Daniel, H., and Young, I. M.: Soil organic carbon mineralization rates in  
920 aggregates under contrasting land uses, *Geoderma*, 216, 10–18, <https://doi.org/10.1016/j.geoderma.2013.10.023>, 2014.

921 Ramos, P., Honda, R., Hoek, E. M. V., and Mahendra, S.: Carbon/nitrogen ratios determine biofilm formation and  
922 characteristics in model microbial cultures, *Chemosphere*, 313, <https://doi.org/10.1016/j.chemosphere.2022.137628>, 2023.

923 Ren, G., Zhang, Y., Chen, Z., Xue, X., and Fan, H.: Research progress of small plant peptides on the regulation of plant growth,  
924 development, and abiotic stress, *Int. J. Mol. Sci.*, 25, 4114, <https://doi.org/10.3390/ijms25074114>, 2024.

925 Renault, H., Alber, A., Horst, N. A., Lopes, A. B., Fich, E. A., Kriegshauser, L., Wiedemann, G., Ullmann, P., Herrgott, L.,  
926 Erhardt, M., Pineau, E., Ehltung, J., Schmitt, M., Rose, J. K. C., Reski, R., and Werek-Reichhart, D.: A phenol-enriched cuticle  
927 is ancestral to lignin evolution in land plants, *Nat. Commun.*, 8, 14713, <https://doi.org/10.1038/ncomms14713>, 2017.

928 Rippin, M., Borchhardt, N., Williams, L., Colesie, C., Jung, P., Büdel, B., Karsten, U., and Becker, B.: Genus richness of  
929 microalgae and Cyanobacteria in biological soil crusts from Svalbard and Livingston Island: morphological versus molecular  
930 approaches, *Polar Biol.*, 41, 909–923, <https://doi.org/10.1007/s00300-018-2252-2>, 2018.

931 Roderic Park, S. E.: Metabolic fractionation of C13 and C12 in plants, *Plant Physiol.*, 36, 133, 1961.

932 San-Emeterio, L. M., Zavala, L. M., Jiménez-Morillo, N. T., Pérez-Ramos, I. M., and González-Pérez, J. A.: Effects of climate  
933 change on soil organic matter C and H isotope composition in a Mediterranean Savannah (Dehesa): An assessment using Py-  
934 CSIA, *Environ. Sci. Technol.*, 57, 13851–13862, <https://doi.org/10.1021/acs.est.3c01816>, 2023.

935 Sánchez-España, J., Mata, M. P., Vegas, J., Lozano, G., Mediato, J., Martínez Martínez, J., Galindo, I., Sánchez, N., del Moral,  
936 B., Ordóñez, B., de Vergara, A., Nieto, A., Andrés, M., Vázquez, I., Bellido, E., and Castillo-Carrión, M.: Leaching tests reveal  
937 fast aluminum fluoride release from ashfall accumulated in La Palma (Canary Islands, Spain) after the 2021 Tajogaite eruption.  
938 J. Volcanol. Geoth. Res., 444, 107959, <https://doi.org/10.1016/j.jvolgeores.2023.107959>, 2023.

939 Schwark, L., Zink, K., and Lechterbeck, J.: Reconstruction of postglacial to early Holocene vegetation history in terrestrial  
940 Central Europe via cuticular lipid biomarkers and pollen records from lake sediments, *Geology*, 30, 463–466,  
941 [https://doi.org/10.1130/0091-7613\(2002\)030<0463:ROPTEH>2.0.CO;2](https://doi.org/10.1130/0091-7613(2002)030<0463:ROPTEH>2.0.CO;2), 2002.

942 La Scola, B., Barrassi, L., and Raoult, D.: A novel alpha-Proteobacterium, *Nordella oligomobilis* gen. nov., sp. nov., isolated  
943 by using amoebal co-cultures, *Res. Microbiol.*, 155, 47–51, <https://doi.org/10.1016/j.resmic.2003.09.012>, 2004.

944 Smith, R. J. L.: Colonization by bryophytes following recent volcanic activity on an Antarctic island, *J. Hattori Bot. Lab.*, 56,  
945 53–63, 1984.

946 Survey Staff, S.: Keys to Soil Taxonomy, 13th ed., edited by: USDA Natural Resources Conservation Service, 2022.

947 Szpak, P.: Complexities of nitrogen isotope biogeochemistry in plant-soil systems: Implications for the study of ancient  
948 agricultural and animal management practices, *Front. Plant Sci.*, 5, <https://doi.org/10.3389/fpls.2014.00288>, 2014.

949 Taddeucci, J., Scarlato, P., Andronico, D., Ricci, T., Civico, R., Del Bello, E., Spina, L., D'Auria, L., Asensio-Ramos, M.,  
950 Calvo, D., Padrón, E., Hernández, P. A., and Pérez, N. M.: The explosive activity of the 2021 Tajogaite Eruption (La Palma,  
951 Canary Islands, Spain), *Geochem., Geophys., Geosyst.*, 24, <https://doi.org/10.1029/2023GC010946>, 2023.

952 Tomašek, I., Damby, D. E., Andronico, D., Baxter, P. J., Boonen, I., Claeys, P., Denison, M. S., Horwell, C. J., Kervyn, M.,  
953 Kueppers, U., Romanias, M. N., and Elskens, M.: Assessing the biological reactivity of organic compounds on volcanic ash:  
954 implications for human health hazard, *Bull. Volcanol.*, 83, <https://doi.org/10.1007/s00445-021-01453-4>, 2021.

955 Troll, V. R., Aulinas, M., Carracedo, J. C., Geiger, H., Perez-Torrado, F. J., V. Soler, Deegan, F. M., Bloszies, C., Weis, F.,  
956 Albert, H., Gisbert, G., Day, J. M. D., Rodriguez-Gonzalez, A., Gazel, E., and Dayton, K.: The 2021 La Palma eruption: social  
957 dilemmas resulting from life close to an active volcano. *Geol. Today*, 40, 96-111, <https://doi.org/10.1111/gto.12472>, 2024.

958 Tseng, H. C., Matsutani, M., Fujimoto, N., and Ohnishi, A.: Draft genome sequence and morphological data of *Planifilum*  
959 *fineticola* PLACP1, a thermophilic chloramphenicol-resistant bacterium isolated from thermophilic sludge, *Data Brief*, 54,  
960 <https://doi.org/10.1016/j.dib.2024.110447>, 2024.

961 Ustiatik, R., Ariska, A. P., Hakim, Q. L., Wicaksono, K. S., and Utami, S. R.: Volcanic deposits thickness and distance from  
962 mt Semeru crater strongly affected phosphate solubilizing bacteria population and soil organic carbon, *J. Ecol. Eng.*, 24, 360-  
963 368, <https://doi.org/10.12911/22998993/170860>, 2023.

964 Valeeva, L. R., Dague, A. L., Hall, M. H., Tikhonova, A. E., Sharipova, M. R., Valentovic, M. A., Bogomolnaya, L. M., and  
965 Shakirov, E. V.: Antimicrobial activities of secondary metabolites from model mosses, *Antibiotics*, 11, 1004,  
966 <https://doi.org/10.3390/antibiotics11081004>, 2022.

967 Valitova, J. N., Sulkarnayeva, A. G., and Minibayeva, F. V.: Plant sterols: Diversity, biosynthesis, and physiological functions,  
968 *Biochemistry (Moscow)*, 81, 819-834, <https://doi.org/10.1134/S0006297916080046>, 2016.

969 Vilhelsson, O., Sigurbjornsdottir, M. A., Thorsteinsdottir, G. V., Cascone, M., Corso, D., Tonietti, L., Migliaccio, F., Nappi,  
970 N., Ricciardelli, A., Selci, M., Montemagno, F., Barosa, B., Bastoni, D., Bastianoni, A., Cordone, A., and Giovannelli, D.:  
971 Diversity of thermophilic prokaryotes, in: *Thermophilic anaerobes. Grand Challenges in Biology and Biotechnology*, edited  
972 by Scully S.M., 21-90, [https://doi.org/10.1007/978-3-031-41720-7\\_2](https://doi.org/10.1007/978-3-031-41720-7_2), 2023.

973 Vilmundardottir, O. K., Sigurmundsson, F. S., Møller Pedersen, G. B., Belart, J. M. C., Kizel, F., Falco, N., Benediktsson, J.  
974 A., and Gisladottir, G.: Of mosses and men: Plant succession, soil development and soil carbon accretion in the sub-Arctic  
975 volcanic landscape of Hekla, Iceland, *Prog. Phys. Geogr.*, 42, 765-791, <https://doi.org/10.1177/0309133318798754>, 2018.

976 Vogts, A., Moosse, H., Rommerskirchen, F., and Rullkötter, J.: Distribution patterns and stable carbon isotopic composition  
977 of alkanes and alkan-1-ols from plant waxes of African rain forest and savanna C3 species. *Org. Geochem.*, 40, 1037-1054,  
978 <https://doi.org/10.1016/j.orggeochem.2009.07.011>, 2009.

979 Volk, M., Bassin, S., Lehmann, M. F., Johnson, M. G., and Andersen, C. P.: 13C isotopic signature and C concentration of soil  
980 density fractions illustrate reduced C allocation to subalpine grassland soil under high atmospheric N deposition, *Soil Biol.*  
981 *Biochem.*, 125, 178-184, <https://doi.org/10.1016/j.soilbio.2018.07.014>, 2018.

982 Wang, H., Wang, J., Xiao, M., Ge, T., Gunina, A., and Jones, D. L.: The fate of amino acid and peptide as affected by soil depth  
983 and fertilization regime in subtropical paddies, *Sci. Total Environ.*, 889, <https://doi.org/10.1016/j.scitotenv.2023.164245>, 2023.

984 Wakeham, S. G., Canuel, E. A.: Biogenic polycyclic aromatic hydrocarbons in sediments of the San Joaquin River in California  
985 (USA), and current paradigms on their formation. *Environ. Sci. Pollut. Res.* 23, 10426-10442, <https://doi.org/10.1007/s11356-015-5402-x>, 2016.

987 Wijesinghe, J. N., Koarashi, J., Atarashi-Andoh, M., Saito-Kokubu, Y., Yamaguchi, N., Sase, T., Hosono, M., Inoue, Y., Mori,  
988 Y., and Hiradate, S.: Formation and mobility of soil organic carbon in a buried humic horizon of a volcanic ash soil, *Geoderma*,  
989 374, <https://doi.org/10.1016/j.geoderma.2020.114417>, 2020.

990 Wygel, C. M., Peters, S. C., McDermott, J. M., and Sahagian, D. L.: Bubbles and Dust: Experimental results of dissolution  
991 rates of metal salts and glasses from volcanic ash deposits in terms of surface area, chemistry, and human health impacts,  
992 *Geohealth*, 3, 338-355, <https://doi.org/10.1029/2018GH000181>, 2019.

993 Yakimov, M. M., Lünsdorf, H., and Golyshin, P. N.: *Thermoleophilum album* and *Thermoleophilum minutum* are culturable  
994 representations of group 2 of the Rubrobacteridae (Actinobacteria), *Int. J. Syst. Evol. Microbiol.*, 53, 377-380,  
995 <https://doi.org/10.1099/ij.s.0.02425-0>, 2003.

996 Yang, Y. R., Guo, Y. X., Wang, Q. Y., Hu, B. Y., Tian, S. Y., Yang, Q. Z., Cheng, Z. A., Chen, Q. J., and Zhang, G. Q.: Impacts  
997 of composting duration on physicochemical properties and microbial communities during short-term composting for the  
998 substrate for oyster mushrooms, *Sci. Total Environ.*, 847, <https://doi.org/10.1016/j.scitotenv.2022.157673>, 2022.

999 Yokobe, T., Hyodo, F., and Tokuchi, N.: Volcanic deposits affect soil nitrogen dynamics and fungal-bacterial dominance in  
1000 temperate forests, *Soil Biol. Biochem.*, 150, <https://doi.org/10.1016/j.soilbio.2020.108011>, 2020.

1001 Yucel, T. B.: Chemical composition and antimicrobial and antioxidant activities of essential oils of *Polytrichum commune*  
1002 (Hedw.) and *Antitrichia curtipendula* (Hedw.) Brid. grown in Turkey, *Int. J. Secondary Metabolite*, 8, 272,  
1003 <https://doi.org/10.21448/ijsm.945405>, 2021.

1004 Zechmeister, H. G., Richter, A., Smidt, S., Hohenwallner, D., Roder, I., Maringer, S., and Wanek, W.: Total nitrogen content  
1005 and  $\delta$  15 N signatures in moss tissue: indicative value for nitrogen deposition patterns and source allocation on a nationwide  
1006 scale, *Environ. Sci. Technol.*, 42, 8661-8667, <https://doi.org/10.1021/es01865d>, 2008.

1007 Zeglin, L. H., Wang, B., Waythomas, C., Rainey, F., and Talbot, S. L.: Organic matter quantity and source affects microbial  
1008 community structure and function following volcanic eruption on Kasatochi Island, Alaska, *Environ. Microbiol.*, 18, 146-158,  
1009 <https://doi.org/10.1111/1462-2920.12924>, 2016.

1010 Zhang, J., Cai, L., Yuan, D., and Chen, M.: Distribution and sources of polynuclear aromatic hydrocarbons in Mangrove  
1011 surficial sediments of Deep Bay, China, *Mar Pollut. Bull.*, 49, 479–486, <https://doi.org/10.1016/j.marpolbul.2004.02.030>,  
1012 2004.